X-RAY STRUCTURE ANALYSIS

OF THIN FILM SOLAR CELL MATERIALS

A THESIS

PRESENTED TO

THE SCHOOL OF GRADUATE STUDIES

ADDIS ABABA

IN PARTIAL FULFILMENT OF THE REQUIREMENTS FOR

DEGREE MASTER OF SCIENCE IN PHYSICS

by

SALAH AHMED

June, 1983

ADDIS ABABA UNIVERSITY

School of Graduate Studies

X-RAY STRUCTURE ANALYSIS OF THIN FILM SOLAR CELL MATERIALS

by

Salah Ahmed

Faculty of Science

Approved by the Examining Board:

Dr. Elaine Girgis Tadros	Elaine G. Tadros
External Examiner	
Dr. H.G. Neumann	H G Neumann
Advisor	
Dr. G. Kluge	G. Kluge
Member	
Dr. V. Davydov	Davydov
Chairman	

ACKNOWLEDGEMENT

I would like to express my sincere gratitude to Dr. H.G. Neumann for the help and guidance from the beginning up to the end in writing this dissertation.

I am also gratefull to Dr. V. Davydov, Dr. J.Jelen and Dr. A. Udris from whose lectures I have benefited much.

I am also grateful to Dr. D. Deininger and Dr. G. Kluge for their encouragements.

I would like also to acknowledge my indebtness to Ato Wodaje Emeru who prepared the glass tubes for the different experiments and Ato Girma Moges for supplying me pure CuCl which was hard to obtain here.

Financial support of the Addis Ababa University is gratefully acknowledged.

TABLE OF CONTENTS

		Page
1	INTRODUCTION	1
2	OPERATION OF PHOTOVOLTAIC CELL	2
	2.1 Recombination Losses	4
	2.2 Current-Voltage Characteristic	6
	2.3 CdS/Cu_xS Thin Film Solar Cells	9
3	THIN FILM DEPOSITION TECHNIQUES	14
	3.1 The Production of Layers of CdS	14
	3.1.1 Thermal Evaporation	14
	3.1.2 Sputtering	15
	3.1.3 Screen-Printed and Sintered Layers	15
	3.1.4 Sprayed Layers	16
	3.1.5 Electrophoretic Deposition . . .	17
	3.1.6 Chemical Spray. Deposition - ion Exchange	17
	3.1.7 Conclusion	18
	3.2 The Formation of Cu_xS Layers	18
	3.2.1 Chemiplating Process (Dipping or Wet Process)	20
	3.2.2 Electroplating Process	21
	3.2.3 Vacuum Deposition Techniques . . .	22
	3.2.4 Solid State Reaction	24
	3.3 Formation SnO_2 Layers	25

Page

4 X-RAY STRUCTURE ANALYSIS 26

4.1. Geometry of Crystals 27

4.1.1 Crystals 27

4.1.2 Lattices 27

4.1.3 Crystal Systems 30

4.1.4 Primitive and Non-Primitive Cells 32

4.1.5 Lattice Direction and Planes 34

4.2. The Intensities of Diffracted Beams 41

4.3. Determination of Crystal Structure 42

4.3.1 Indexing Pattern of Cubic Crystals 44

4.3.2 Indexing Pattern of Tetragonal Crystals (Graphical Method) . 47

4.3.3 Indexing Pattern of Hexagonal Crystals (Graphical Method) . 51

4.4 X-Ray Diffraction 53

4.4.1 Counter Diffractometer 53

4.4.1.1 Diffractometer Geometry . . . 53

4.4.1.2 Specimen 54

4.4.1.3 X-Ray Optics 56

4.4.1.4 Recording Diffracted Radiation 59

5. EXPERIMENTAL PROCEDURE 59

5.1 Apparatus Used for X-Ray Diffraction 59

5.2 Preparation of Thin Films 60

5.2.1 CdS Films 60

5.2.2 Cu_xS Films 64

Page

5.2.3 SnO_2 Films 65

5.3 Analysis of the Structure of Thin Films Prepared 65

5.4 Experimental Results and Discussion . 66

5.4.1 CdS Films 66

5.4.1.1 Screen-Printed Films 66

5.4.1.2 Evaporated Films 70

5.4.1.3 Conversion of CdO into CdS . . 77

5.4.2 Cu_xS Films 84

5.4.3 SnO_2 Films 93

6. CONCLUSION AND OUTLOOK 95

7. REFERENCES 97

LIST OF TABLES

		Page
1.	Symmetry and lattice constants of CdS and various copper sulphides	11
2.	Lattice parameters of CdS and Cu_2S	13
3.	Crystal systems and Bravais lattices	31
4.	Condition for reflection and extinction for different lattices types.	42
5.	X-ray powder data for cadmium sulphide	67
6.	X-ray powder data for digenite	87
7.	X-ray powder data for CuCl	87
8.	X-ray powder data for $CuCl_2$	88
9.	X-ray powder data for $Cu_{1.96}S$	88
10.	X-ray powder data for chalcocite	93
11.	X-ray powder data for cassiterite.	94

LIST OF FIGURES

		Page
1.	Cu_2S elementary cell ⊥ c cut and its lattice mismatch to CdS.	12
2.	A point lattice	29
3.	A Unit cell	30
4.	Face-centerd cubic point lattice referred to cubic and rhombohedral cells	33
5.	Indices of directions	35
6.	Plane designation by Miller indices	36
7.	The hexagonal unit cell and indices of planes and directions	37
8.	Two-dimensional lattice	38
9.	Plot of $d_{hk\ell} = (h^2+ k^2+\ell^2)^{-\frac{1}{2}}a$ for each possible combination of h, k and ℓ	46
10.	Partial Hull-Davey chart for a simple tetragonal system.	49
11.	Partial Hull-Davey chart for hexagonal crystals	52
12.	Basix focusing geometry of the used diffractometer	55
13.	Experimental arrangement of the furnace used for sintering and its temperature profile	61
14.	Experimental arrangement for the vapour deposition of CdS films.	62
15.	Experimental arrangement for sulphidation of CdO films.	63

Page

16. Experimental setup for solid state reaction 64

17. XRDP of a screen-printed CdS film on SnO_2-coated glass slide. 68

18. XRDP of SnO_2-coated glass slide. 69

19. XRDP of evaporated CdS film on SnO_2-coated glass slide. 72

20. XRDP of evaporated CdS film from a mixture of CdS and $CdCl_2$ on a glass slide. 73

21. XRDP of evaporated CdS film after a certain heat treatment. 74

22. XRDP of evaporated CdS film after additional heat treatment. 75

23. XRDP of evaporated CdS film on a heated glass slide. 76

24. XRDP of a vapour deposited and partly oxidized Cd film. 78

25. XRDP of a vapour deposited and oxidized Cd film. 79

26. XRDP of a CdS film 80

27. XRDP of evaporated CdO film on a glass slide. 81

28. XRDP of a vapour deposited CdO film by evaporation of cadmium acetate on a heated glass. 82

29. XRDP of Cu_xS films on CdS films by solid state reaction 86

30. XRDP of $CuCl/CuCl_2$ powder, which has been used as an evaporant for CuCl layer deposition . . 89

Page

31. XRDP of the $CuCl/CuCl_2$ layer for solid state reaction. 90

32. XRDP of the $CuCl/CuCl_2$ layer for solid state reaction after reduction of the evaporant. . . 91

33. XRDP of a screen printed CdS layer, partly converted to Cu_xS by solid state reaction with an evaporated $CuCl/CuCl_2$. 92

ABSTRACT

X-ray diffractometery is used for studying the crystalline structure of thin film CdS/Cu_xS (where x is slightly less than or equal to 2) solar cell materials. The different films prepared are CdS, Cu_xS, and SnO_2. The CdS films are prepared by:

a) screen printing of a mixture CdS, $CdCl_2$ (used as a flux) and propane 1 - 2 diol (used as a binder) on a glass slide and then sintering at a pressure of about 80 Pa at a temperature of around 640°;

b) evaporation of a mixture of CdS and $CdCl_2$ at a pressure of about 80 Pa and deposition on glass substrates at temperatures between 300 and 500°C;

c) chemical vapour deposition of CdO on glass slides and conversion of this CdO film into CdS at a temperature of 500°C by an ion exchange reaction on passing H_2S.

Only in case (b) the desirable (001) textured (c⊥ to substrate surface) CdS layers are obtained.

The Cu_xS films are prepared by a solid state reaction. CuCl/$CuCl_2$ (mixture: CuCl oxidizes easily to $CuCl_2$ upon exposure to air) films were deposited on a CdS film by evaporation of CuCl/$CuCl_2$ (mixture) powder at vacuum of 80 Pa. For a substrate temperature of about 500°C the solid state reaction between

$CuCl/CuCl_2$ (mixture) and CdS and the evaporation of produced $CdCl_2$ occurs simultaneously. The obtained Cu_xS modifications are $Cu_{1,8}S$, $Cu_{1,96}S$ and Cu_2S. The x-value in this modifications increases with decreasing of the amount of $CuCl_2$ in the mixture. Because of the high reaction temperature the high temperature modification of the $Cu_{1,96}S$-phase is produced.

The SnO_2 films are prepared by chemical vapour deposition of $SnCl_2$ in air. The crystalline structure is as expected tetragonal.

The x-ray diffraction pattern (XRDP) are obtained by means of a Norelco Wide Range Diffractometer coupled with a Philips x-ray generator (XRG 3000) with a copper target tube. The patterns are indexed by referred intensity and lattice information. The method being nondestructive, has the advantage of obtaining information at all stages of fabrication of the thin films, hence, the effects of process pertubation can be studied such that it is possible to suggest the best method of obtaining desirable thin films for efficient solar cells.

1. INTRODUCTION

The photovoltaic solar cell is a semiconductor device which converts sunlight directly into electricity. The operation of this device is based on the photovoltaic effect which is the conversion of light energy (photons) to electrical energy in a semiconductor junction device. The photovoltaic effect has been observed since 1839 and the theory has been developed since 1930. The importance of solar cells for the space program has led to further refinement of the analysis which allows their performance to be predicted within 10 percent efficiency.

Solar cells consist of thin sandwich of one or more semiconductors, with metal electrodes on either side. A transparent coating envelopes the device to shield it from harmful effects of the atmosphere and to assist the absorption of light. Cells made of monocrystalline semiconductors, although very thin, are stiff and inflexible. Cells made of thin-film polycrystalline or amorphous semiconductors can be rolled and unrolled like conventional roofing materials.

A photovoltaic effect in CdS was first observed by Reynolds made by depositing a thin film of copper on a cadmium sulphide film/1/. Later work established that the actual junction was

between CdS and Cu_2S /2/. A substantial number of research efforts have since been conducted on this heterojunction and although some variation exists, cells have generally been made by reacting a vapour deposited cadmium sulphide with a cuprous ion solution.

The object of this study is to produce thin films for CdS/Cu_2S solar cells and to investigate their crystalline structure by x-ray diffraction.

2. OPERATION OF PHOTOVOLTAIC CELLS /3/

The photovoltaic effect is the creation of an electromotive force (EMF) by absorption of light or any ionizing radiation in an inhomogeneous solid. It is distinguished from localized heating which can cause an EMF via thermoelectric effects or from nonuniform illumination in a homogeneous sample.

In order for the photovoltaic effect to exist in the system, the light must generate charge carriers, both electrons and holes, which must be separated by an electric field created by some electronic inhomogeneity which is generally called the electronic junction and is described by a change in the energy level of the conduction band relative to the Fermi level.

The electronic junction, necessary for the photovoltaic device, can be the region between two semiconductors having different types of conductivity hence comprising a p-n junction which can be:

a homojunction which has the same semiconductor on both sides of the junction,

a heterojunction composed of two different semiconductors,

a Schottky-barrier metal-semiconductor junction,

a metal-insulator-semiconductor (MIS) junction.

The essential features of a solar cell are an absorber material in which mobile carriers are generated by the absorption of light, and build-in voltage region which allows the generated carriers to be collected from the region in which they are generated and converted to majority carriers. The absorber region determines the magnitude of the current that is generated and the height of the barrier voltage determines the voltage that the cell can produce. Absorption of light by the semiconducting absorber requires, that the light energy is at least equal in magnitude to that of the energy gap separating the valency band from the conduction band (band gap). A fraction of light having the proper energy can be lost if the

semiconductor layer is not thick enough to effect complete light absorption (ie. thinner than the optical absorption length of the semiconductor).

2.1 Recombination Losses

Losses due to photogenerated electrons and holes recombining before they are separated in the p-n junction are highly influenced by the material quality and device structure. Bulk recombination takes place away from surfaces and interfaces and generally occurs at impurity sites and structural defects in the semiconductor. Since most carriers are generated in the bulk, outside the junction, minimizing bulk recombination results in a big fraction of photogenerated carriers migrating to the junction so as to be separated. It means the diffusion length (the distance photogenerated carriers diffuse without recombination) has to be long enough to allow all carriers to reach the junction. In addition, weakly absorbing materials require longer diffusion length for efficient carrier collection.

Other effective recombination centers arise due to unique electronic states which arise in the vicinity of compositional and structural discontinuities in the solids (or in all active and passive parts of the solar cell). Hence,

surfaces and interfaces are critical regions in the solar cell. Surface recombination is particularly important in p-n homojunctions, where many carriers are generated in the front active element. In this type of cells the effect can be minimized by decreasing the thickness of the front active element or addition of a compatible transparent semiconductor layer in front of the cell (heterostructure).

In heterojunction cells the front active element can be made of a semiconductor with a wide band gap which will only absorb the small fraction of the incident radiation of energy larger than the band gap. Hence, most carriers are generated in the back active element and thus are not susceptible to front surface recombination.

Recombination at the back side becomes appreciable when the thickness of the back active element is comparable to both the optical absorption length of the semiconductor and the carrier diffusion length. It is because an appreciable number of carriers are generated near the back surface, where the recombination rate is high. This effect can be reduced by using a back-surface field structure, in which the region of the back active element adjacent to the electrodes is heavely doped. Consequently a field is produced that effectively confines the photocarriers to

the bulk of the back active element and the photocarriers are kept away from the electorde.

Defects arising at the interface between two dissimilar materials provide another important recombination path. Interface recombination is an important loss mechanism in heterojunctions and Schottky barriers and is reduced by matching certain key properties of the materials envolved such as lattice parameter, thermal expansion, energy of the conduction and valency band edges, etc. Another interface highly affecting efficiency is found at grain boundaries of polycrystalline materials.

2.2 Current-Voltage Characteristic /3/.

A semiconductor junction has the electrical characteristic of a diode, ie. significant current flows only for one polarity of applied voltage. This forward polarity is precisely the one appearing across an illuminated cell connected to a load. The current thus produced, the diode current, flows in the direction opposite to the photogenerated current under short circuit conditions. The net current flow is therefore reduced from that under short-circuit conditions by the magnitude of this diode current and becomes

zero when the load resistance becomes infinity. This is called the open-circuit condition, and the voltage measured under this condition is the one at which the diode current exactly balances out the photocurrent. Consequently high open-circuit voltages are obtained for small diode current.

The magnitude of the diode current for a given voltage bias and polarity depends on the current-carrying mechanism across the junction. When current is carried only by diffusion of energetic carriers over the top of the potential barrier at the junction, the diode current is a minimum and the open-circuit voltage is a maximum. Voltage of forward polarity reduces the height of this barrier and increases the diode current and if it is large enough, the barrier vanishes and the diode current can balance any photocurrent produced by the cell.

For homojunctions the maximum open circuit voltage acheivable is slightly smaller than the band gap of the semiconductor. Hence, the use of large band gap semiconductors produce high voltages. But such semiconductors produce small current due to their absorbing less radiation.

The power delivered by a cell to the load is equal to the product of the current and the voltage across the cell and therefore depends on the load. When the load is zero or infinite the power delivered is zero. For some finite load resistance the power reaches a maximum.

The efficiency of solar cells is influenced by electorde design, contact fabrication and electrical shorts across active elements. These effects can be described in terms of an added series resistance between cell and load, which has to be minimized or a shunt resistance across the cell terminals which has to be maximized for efficient cell operation. The front electrode is either a transparent continuous layer or a fine grid structure with minimum shading so as to maximize the amount of solar radiation reaching the active element. Electrode light transmission is usually improved at the expense of increased resistance, leading to the reduction of efficiency. Increasing the conductivity of transparent electrode or active elements, therefore, improves device performance.

Another important factor to cell efficiency is cell stability over many years of exposure to sunlight and other environmental stresses.

2.3 CdS/Cu_xS Thin Film Solar Cells /5,6/.

CdS/Cu_xS thin film solar cells are one of the most investigated photovoltaic devices. The first thin film cell was developed by Carlson /4/ and, after 1960, conversion efficiences of greater than 1% were reached. Intensive development produced cells of relatively large area ($55cm^2$) with mean efficiencies of about 6%, some cells of 4 cm^2 having efficiencies of over 8%.

However, several problems appeared and these increased in number as the efficiency of the cells increased. The main problem was the low yield of efficient cells, and the dependence of the performance on the preparation method. As the photovoltaic mechanism and the structure of the junctions were not understood, the improvments made to the cells were essentially empirical and all these cells were very sensitive to different degradation mechanisms.

The principal difficulty in achieving higher efficiencies seems to lie in reducing substancial CdS/Cu_xS interface recombination. The analysis of the chemistry of this interface enables one to estimate the recombination velocity at the CdS/Cu_xS heterojunction and to see which other consequences for the band structure near the interface result. This analysis is based on the lattice mismatch (at the junction) and related space charges.

Copper sulphide can exist in a large number of phases (see Table 1 and Chapter 3.2), but a useful phtovoltaic effect has been observed for the chalcocite phase (Cu_2S). Cu_2S is usually produced on top of the CdS layer by a topotaxial reaction, that is, replacing a cadmium ion by two copper ions, but leaving the sulphur sublattice essentially intact. The lattice structure changes slightly from the hexagonal CdS with a = 4.1368 Å and c = 6.7162 Å to the orthorhorbic Cu_2S with a = 11.976 Å, b = 27.640 Å, c = 13.488 Å. Generally the lattices are macroscopically connected in a plane perpendicular to c (see Chapter 4). Fig.1 shows a cut through a sulphur layer at the CdS/Cu_2S interface perpendicular to the c axis (of both CdS and Cu_2S) as an example.

The mismatch between the chalcocite and the CdS lattice shown which is the smallest for all of the possible crystallographic phases of Cu_xS, (Table 2) produces a dislocation network with an excess sulphur layer in the Cu_xS at a distance of 52.9, 96.7 and 808.8 Å in the a,b and c direction respectively. This extra layer provides a line network of dangling bonds with a density of 3.44×10^{13}, 6.25×10^{13} and 1.07×10^{14} cm^{-2}, perpendicular to the a, b and c direction, respectively.

It is expected that all of these dangling bodns are (relative to the lattice) negatively charged, and attract compensating charges (donors) in the adjacent CdS and Cu_xS. A higher donor density is expected in Cu_xS, caused by Cd interstitials trapped during the topotaxial Cu_xS formation. These donors provide a high density of donor-acceptor pairs with enhanced recombination and decrease the efficiency of the photovoltaic cell (see Chapter 2.1).

Table 1 Symmetry and lattice constants of CdS and various copper sulphides /2,5/.

Compound	Crystals Structure	Lattice Constants /Å		
		a	b	c
CdS	Hexagonal	4,137		6,716
Cu_2S	Orthorhombic	11,976	27,640	13,488
Cu_2S	Hexagonal	3,961		6,722
$Cu_{1.96}S$	Orthorhombic	15,71	13,56	26,84
$Cu_{1.96}S$	Tetragonal	4,008		11,268
$Cu_{1.91}S$	Hexagonal	11,355		13,506
$Cu_{1.8}S$	Pseudocubic	5,56		
CuS	Hexagonal	3,794		16,332

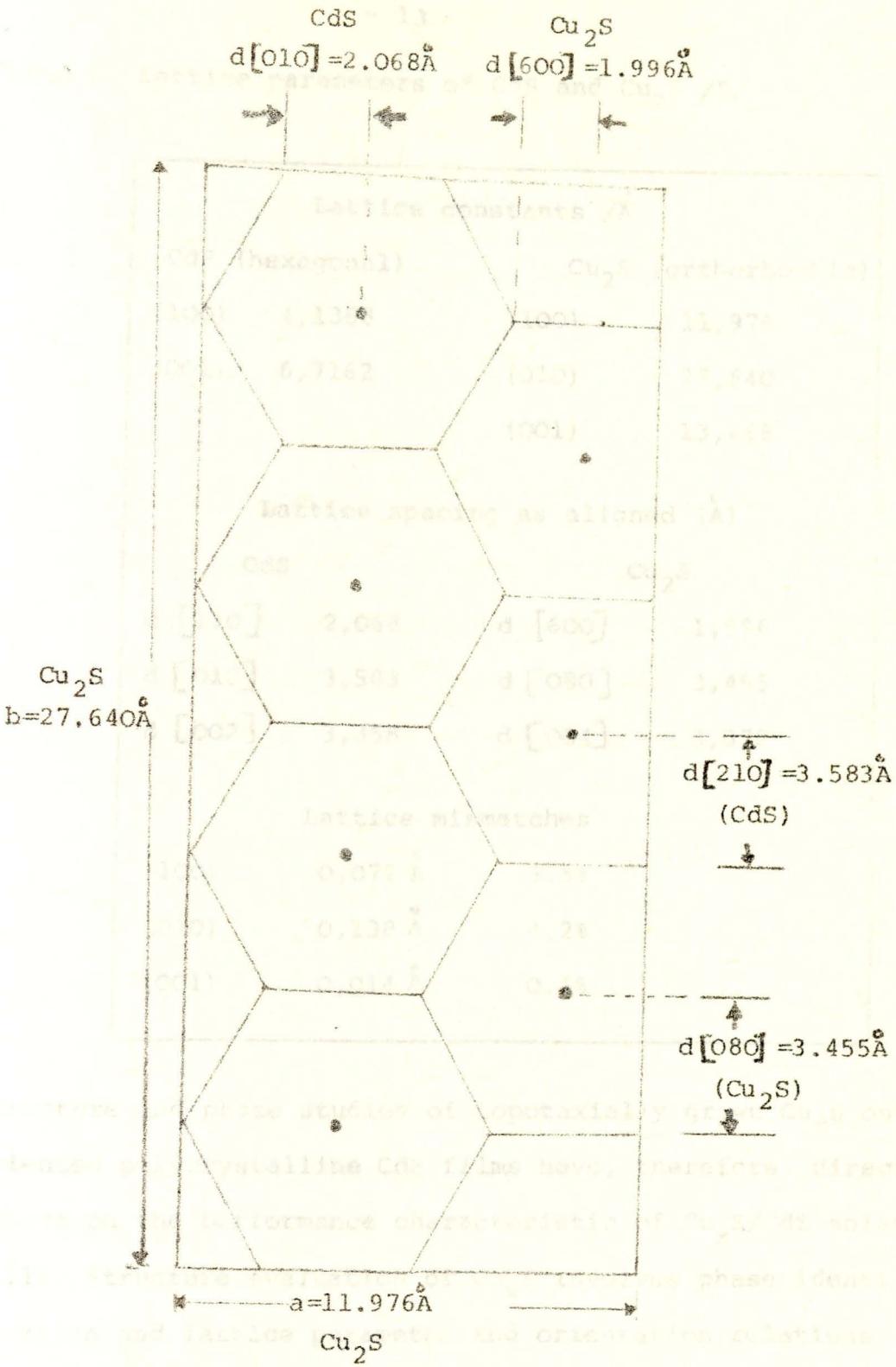


Fig.1. Cu_2S elementary cell $\perp$ c cut (approximate). Sulphur layer depicted. Lattice mismatches to CdS lattice indicated.

Table 2 Lattice parameters of CdS and Cu_2S /5/

Lattice constants /Å			
CdS (hexagonal)		Cu_2S (orthorhombic)	
(100)	4,1368	(100)	11,976
(001)	6,7162	(010)	27,640
		(001)	13,488
Lattice spacing as aligned (Å)			
CdS		Cu_2S	
d [110]	2,068	d [600]	1,996
d [010]	3,583	d [080]	3,455
d [002]	3,358	d [004]	3,372
Lattice mismatches			
(100)	0,072 Å	3.5%	
(010)	0,138 Å	4.2%	
(001)	0,014 Å	0.4%	

Structure and phase studies of topotaxially grown Cu_xS on oriented polycrystalline CdS films have, therefore, direct impact on the performance characteristic of Cu_xS/CdS solar cells. Structure evaluation of Cu_xS involves phase identification and lattice parameter and orientation relations to get a meaningful interpretation of stoichiometry.

3. THIN FILM DEPOSITION TECHNIQUES

3.1 The Production of Layers of CdS

CdS layers are invariably n-type as a consequence of the presence of a large density of native defects (sulphur vacancies and excess cadmium) which act as donors.

3.1.1 Thermal Evaporation /7/.

One of the most common techniques for the deposition of CdS thin films is the thermal evaporation. The obtained polycrystalline layers show a columnar structure with the c axis perpendicular to the substrate surface if the substrate is heated at 200°C during deposition. These layers exhibit a large number of pinholes and need a thickness of up to a few tens of microns to avoid short circuits in the complete cell. The size of crystallites is about 1 μm, and their c axis is approximately normal to the substrate. To produce low resistance films (which are needed for solar cells) the easiest way is to introduce donor native defects (sulphur vacancies) or donor impurities (indium).

The main disadvantage of this method is that 80% of the evaporated material is lost.

3.1.2 Sputtering /7,8,9/.

By using sputtering, over 80% of the material sputtered from the target can be deposited onto a substrate, the uniformity of the orientation of the c axis is greatly improved, and the density of pinholes is considerably reduced.

The properties of the sputtered layers are quite similar to those of the evaporated films except for the resistivity which is typically 1 M Ω cm for layers condensed on substrates heated at 200°C, probably as a result of better stoichiometry.

The main disadvantage of this method is the difficulty of doping and the low deposition rate (about 2 µm/h).

3.1.3 Screen-Printed and Sintered Layers /10/.

CdS films of low resistivity are prepared by screen-printing a CdS paste on a glass substrate and then sintered in N_2 gas atmosphere including a small amount of Cd vapour. The CdS paste is prepared by mixing 100 g CdS powder and 7 g $CdCl_2$ powder (flux) with propylene glycol (binder). The printed paste is then sintered at 640°C for one h. The resistivity of these films is 10^{-2} Ω cm with grain sizes of 5 - 10 µm for a thickness of about 50 µm.

3.1.4 Sprayed Layers /7,11,12/

An aqueous solution of a cadmium salt and a sulpho-organic compound is sprayed onto a heated substrate whose temperature is above 250°C. The reaction which develops on the hot substrate produces a CdS layer and volatile products. With the commonly used $CdCl_2$ and thioria $SC(NH_2)_2$, the global reaction is

$$CdCl_2 + SC(NH_2)_2 + 2H_2O \rightarrow CdS + 2NH_4Cl\uparrow + CO_2\uparrow$$

The spray can be realized in N_2 atmosphere and the sprayed layers are more compact and stoichiometric than the evaporated films, so the CdS thickness may be reduced below 10 µm. The deposition rates are rather low with values around a few microns per hour. For substrate temperatures less than about 300°C, the layers are very rough, with small disoriented crystallities. Above 350°C the layers resemble evaporated layers in many aspects: they are smoother, with a crystallite size of about 0.1 µm, have an acceptable c axis alignment normal to the substrate and are optically transparent.

3.1.5 Electrophoretic Deposition /14/.

The preparation of pinhole-free thin films of CdS by the above mentioned methods has always been a problem. Electrophoresis from a CdS sol offers an alternative technique. Provided the particle size is small enough, pinhole-free films 1-2 μm thick can be prepared on large-area substrates. The sol was prepared by bubbling H_2S into a solution of cadmium acetate and water. A particle size of about 100 Å was used so that no additives were required to prevent the sol flocking out. The sol was stable for periods of many weeks when kept in darkness. This particle size also meant that pinhole-free films 1 μm thick could be prepared.

3.1.6 Chemical Spray Deposition-Ion Exchange /15/.

First films of CdO which are 1-3 μm thick are deposited by spray pyrolysis of cadmium acetate or cadmium nitrate on SnO_2 or In_2O_3 coated glass slides, maintained at temperatures between 450 and 550°C. These films are subjected to an ion exchange procedure in a flowing sulphide ambient at temperatures of 400-500°C. These films are completely converted into CdS. The CdS films, now 2-6 μm thick, have grain diameters of 1-3 m. It is important to note that even though the two phases have significantly different densities and crystal structures, the converted CdS films

remain intact and adherent to the substrate. Specifically, CdO crystallizes in the cubic rock salt structure with a density of 8.15 g/cm^3, while CdS has the hexagonal wurtzite structure with a density of 4.82 g/cm^3. The total number of molecules present in the film remains constant during the transformation, and the molecular weight increases by only 12%, but the density decreases by almost a factor of 2. Thus, the volume of the film is doubled. The lateral expansion is taken up by the filling of voids between the original CdO crystallites, while the upward expansion acually serves to increase the film thickness.

3.1.7 Conclusions

All the methods described are able to produce suitable CdS layers for solar cell preparation. There are preparation techniques such as organometallic chemical vapor deposition /13/, solution growth /16/; however, only preliminary results are currently available.

3.2 The Formation of Cu_xS Layers.

Several copper sulphides are known /2, Table 1/. Crystal structures of several of the phases have been studied; there is a general agreement on the locations of the sulphur atoms. The structures appears to divide into two groups,

that based upon hexagonal arrangement of sulphur atoms such as found in hexagonal Cu_2S and CdS (Fig. 1), and that based upon a cubic closely packed arrangement of the sulpher atoms such as is found in diginite and cubic CdS.

The different crystallographic phases of Cu_xS are chalcocite (Cu_2S), which transforms from orthorhombic pseudo-hexagonal to hexagonal at 103°C and to cubic at 435°C; djurileite ($Cu_{1.96}S$), which is orthorhombic and appears to transform sluggishly to a metastable tetragonal form, above 93°C ; diginite ($Cu_{1.855}$), which is pseudo-cubic below and cubic above ~ 80°C; and covellite (CuS), which decomposes above 507°C; and of these crystallographic phases only the chalcocite phase has proved to tbe the optimal composition for high photoelectric conversion efficiency in CdS/Cu_2S photovoltaic ecells.

Cu_2S is generally a p-type degenerate material due to copper vacancies, with an energy gap of 1.2 eV. It has a very marked optical absorption especially along the c axis. Diffusion length for electrons of about 0.3 µm are usaully found. A general problem connected with the various methods of formation of this Cu_xS layer is the stoichiometric composition ($x = 2$). In studying the effect of aging on Cu_2S it was shown (/2/ that the crystals tend to

shift to lower copper content. The mobile copper atoms migrate to the surface of the crystals and oxidize there. This suggests the necessity of rigidly controlling the preparation conditions when one is working with copper sulphides.

3.2.1 Chemiplating Process (Dipping or Wet Process) /7,17,18/.

A film of CdS is dipped in a hot (about 90°C) solution of CuCl with a carefully controlled pH value (of about 4) and the global reaction is

$$CdS + 2CuCl \Rightarrow Cu_2S + CdCl_2$$

The reaction proceeds quickly, producing about 0.3 µm of Cu_2S in a few seconds.

The CdS surface is etched with HCl acid before dipping in order to present a clean fresh CdS surface to the Cu Cl solution. Apart from presenting a fresh CdS surface, the etching also increases the area of the junction between the CdS and the Cu_xS and enhances the penetration of the Cu_xS into the CdS grain boundaries.

In order to improve the stoichiometry of the Cu_xS, additional treatment is done to obtain the $Cu_{1.995}S$ composition, which is found to give useful photovoltaic effect.

This method produces oriented layers suitable for cell preparation because a topotaxial growth occurs during the exchange reaction.

3.2.2 Electroplating Process /10/.

A CdS layer is etched with HCl, and then immersed, together with a copper plate, in an aqueous solution of $CuSO_4$. A direct current voltage is applied between the copper plate (anode) and the CdS film (cathode) within the deposition potential of metallic copper at 20°C for 1 hour. A Cu_xS layer is formed on the surface and along the grain boundaries near the surface of the CdS film according to the following reactions:

$$Cu^{++} + CdS \Rightarrow CuS + Cd^{++}$$

$$CuS + (x-1)Cu^{++} + 2(x-1)e \Rightarrow Cu_xS$$

Here Cu_xS represents the mixture of Cu_2S , $Cu_{1.96}S$ and $Cu_{1.8}S$ phases. Thus, a film of Cu_xS is formed on the surface of the CdS film.

3.2.3 Vacuum Deposition Techniques

All vacuum deposition techniques produce Cu_xS layers independently of the CdS substrate, but their main disadvantage lies in the misorientation of the films because of the absence of topotaxy. The first tentative results were layers of poor stoichiometry because of dissociation of the compound. Flash evaporation gives better results. During the last 4 years, sputtering has been used successfully for the preparation of Cu_xS layers /8,9/. Thin films of Cu_xS (0.3-0.5 µm thick) were produced by r.f. sputtering using hydrogen and H_2S as additives to the sputter gas argon. The electrical resistivity and the optical properties of the films show marked changes when the concentration of the reactive part of the sputter gas exceed 1%. These changes correspond to a variation in the chemical composition of the Cu_xS layers. The films are polycrystaline and consist of a mixture of crystallographic phases that are not in thermodynamic equilibrium in all of the sputtered layers.

A new technique , namely organometallic chemical vapour deposition /13/, has been developed. This method can deposite Cu_2S layers and has a better control over the Cu_2S stoichiometry, and it can also provide a precise means in the control of the doping level and type of dopants.

The main consideration in the choice of copper compounds as sources for the CVD process is their vapour pressure. Sufficient vapour pressures of these compounds at relatively low temperatures are required for the process to succeed. There are very few copper compounds that fit such requirement. In this work, vapour of $\left[CuCl(NCCH_3)\right]_n$ was used as the copper source, which was generated by bubbling nitrogen through the sources, in which acetonitride was used as a solvent and the following reaction is held:

$$n(Cu_2Cl_2) + n(CH_3CN) \Rightarrow \left[(CuCl(NCCH_3)\right]_n$$

For the sulphur source, dry H_2S gas was used.

A horizontal heating reactor system is used. Growth of Cu_2S is obtained over a wide range of temperatures and gas compositions. The reactor temperature was set between 600-900°C and the carrier-gas-flow (N_2) was set between 0.05-0.2 cm^3/min; the H_2S gas flow was set between 0.01-0.03 cm^3/min.

In all cases, the growth rate of films was found to increase with the substrate temperature, the growth rate was negligibly small when the reactor temperature was 700°C and reasonable growth rate was obtained when this temperature was 800°C.

The as grown layers are black in color, and the surfaces are mirror-like. X-ray diffraction was used to examine the phases of the films. From this it was concluded that the produced Cu_xS-phase is chalcocite.

Since the above mentioned deposition techniques are in the preliminary stage, further investigation along these lines is necessary.

3.2.4 Solid State Reaction /19/.

This method combines the advantages of vacuum deposition and of the exchange reaction to produce topotaxial films of Cu_xS on CdS layers. The junction develops in the CdS as for the wet process, and does not result from the sticking of two different materials as for vacuum deposition. The method consists in the evaporation of the CuCl onto a CdS layer with subsequent heat treatment to produce the same chemical exchange reaction of that for the chemiplating process. The two films are then backed in an inert or reducing atmosphere at about 180-200°C for a few seconds. The unreacted CuCl and the $CdCl_2$ produced are washed off the free surface using alcohol.

Structural data suggest a topotaxial growth of Cu_xS, and the reaction is limited to few tenths of a micron without deep penetration into the grain boundaries of the CdS layer.

The main problem is the evaporation of carefully purified CuCl (without $CuCl_2$) and the limited thickness of the Cu_xS which occurs probably because of the formation of an impermeable layer or $CdCl_2$ during the exchange reaction/7/.

3.3 The Formation of SnO_2 Layers /20,21/.

Tin oxide films have been reported by many investigators as transparent conducting films. SnO_2 is an extrinsic n-semiconductor. SnO_2 films were deposited for several minutes onto a surface of a preheated (450°C) glass slide by chemical vapour deposition of $SnCl_2$ in air.

4. X-RAY STRUCTURE ANALYSIS /22, 23, 24/.

X-rays are electromagnetic radiation which have wavelengths comparable with the interatomic spacings within the crystal. When x-rays strike a crystal, some of the incoming radiation is scattered by electrons of the atoms in the crystal. The radiation scattered from periodically spaced atoms adds coherently to produce diffracted beams for certain incident directions.

W.L. Bragg was able to account for the angles at which the diffracted beams are observed. His analysis showed that the diffracted beam and the incident beam make the same angle with a set of equally spaced parallel planes of the crystal atoms. The different planes of the crystal then act as a kind of partially reflecting 'mirrors'.

The condition which must be met in order that the 'reflected' beams add constructively to yield an intense diffracted beam is that they all be in phase. This condition, known as Bragg's Law, is expressed by:

$$2d \sin \Theta = n \lambda \qquad n = 1,2,3... \qquad (1)$$

where d is the spacing between the planes, Θ is the angle which the incident beam makes with the planes and λ the

wavelength of the electromagnetic radiation. As the index of refraction of x-rays is essentially unity, the transmitted beam therefore passes through the crystal unrefracted.

4.1 The Geometry of Crystals

4.1.1 Crystals

A crystal may be defined as a solid composed of atoms arranged in a pattern periodic in three dimension. As such, crystals differ in a fundamental way from gases and liquids because of the atomic arrangements in the latter which do not posses the essential requirements of periodicity. Not all solids are crystalline, however; some are amorphous, like glass and do not have any regular interior arrangement of atoms.

4.1.2 Lattices

In thinking about crystals it is often convenient to ignore the actual atoms composing the crystal and their periodic arrangement in space, and to think instead of a set of imaginary points which have fixed relation in

space to the atoms of the crystal and may be regarded as a sort of frame work or skeleton on which the actual crystal is built up.

These points can be formed by intersection of three parallel and equidistant sets of planes. The set of points so formed has an important property; it constitutes what is called a point lattice, which is defined as an array of points in space so arranged that each point has identical surrounding.

By identical surrounding it is meant that the lattice of points, when viewed in a particular direction from one lattice point, would have exactly the same appearance when viewed in the same direction from any other lattice point. The set of cells produced by the intersection of the above planes are identical (in shape and size) and one of them is called a unit cell.

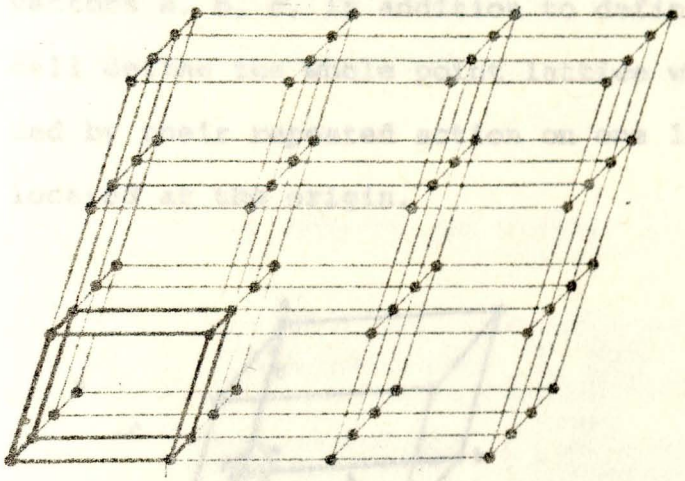


Fig. 2 A point lattice

The size and shape of a unit cell in turn can be described by three vectors $\vec{a}$, $\vec{b}$ and $\vec{c}$ drawn from one corner of the cell taken as the origin. These vectors define the cell and are called the crystallographic axes of the cell. They may also be described in terms of their lengths (a, b, c) and the

the angles between them (α, β, γ) which are collectively called lattice parameter of the unit cell. The vectors $\vec{a}$, $\vec{b}$, $\vec{c}$, in addition to defining the unit cell define the whole point lattice which is produced by their repeated action on one lattice point located at the origin.

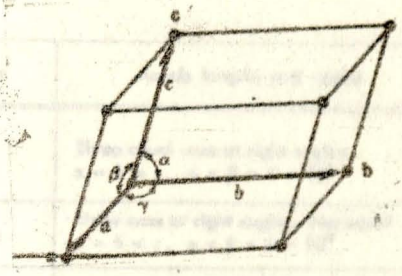


Fig.3 A unit cell

4.1.3 Crystal Systems

In dividing space by three sets of parallel planes, one can of course produce unit cells of various shapes, depending on how the planes are arranged. By giving special values to the axial lengths and angles to the so produced unit cells one comes up with units cells of various kinds of point lattices, since the points of the lattice are located at the

cell corners. It turns out that only seven different kinds of cells are necessary to include all the possible point lattices. These correspond to seven crystal system into which all crystals can be classified. These systems are listed in Table 3.

Table 3. Crystal systems and Bravais lattices/24/.

System	Axials lengths and angles	Bravais lattice	Lattice symbol
Cubic	Three equal axes at right angles $a = b = c$, $\alpha = \beta = \gamma = 90^\circ$	Simple Body-centered Face-centered	P I F
Tetragonal	Three axes at right angles, two equal $a = b \neq c$, $\alpha = \beta = \gamma = 90^\circ$	Simple Body-centered	P I
Orthorhombic	Three unequal axes at right angles $a \neq b \neq c$, $\alpha = \beta = \gamma = 90^\circ$	Simple Body-centered Base-centered Face-centered	P I C F
Rhombohedral*	Three equal axes, equally inclined $a = b = c$, $\alpha = \beta = \gamma \neq 90^\circ$	Simple	R
Hexagonal	Two equal coplanar axes at 120°, third axis at right angles $a = b \neq c$, $\alpha = \beta = 90^\circ$, $\gamma = 120^\circ$	Simple	P
Monoclinic	Three unequal axes, one pair not at right angles $a \neq b \neq c$, $\alpha = \gamma = 90^\circ \neq \beta$	Simple Base-centered	P C
Triclinic	Three unequal axes, unequally inclined and none at right angles $a \neq b \neq c$, $\alpha \neq \beta \neq \gamma \neq 90^\circ$	Simple	P

* Also called trigonal.

In addition to producing the seven different point lattices by simply putting points at the corners of a unit cell of the seven crystal systems, there are

other arrangement of points which fulfill the requirements of the point lattice (namely that each point has identical surroundings). The French crystallographer Bravais worked out the problem and in 1848 demonstrated that there are fourteen possible lattices and no more. The fourteen point lattices or Bravais lattices are described in Table 3. The syrbols P,F,I, etc. have the following meanings. P stands for the so called primitive cell where the unit cell has only one lattice point per cell. F,I etc. which stand for non primitive unit cells and have more than one lattice point per cell. A lattice point in the interior or a cell "belongs" to that cell, while one in a cell face is shared by two cells and one at the corner is shared by eight cells.

4.1.4 Primitive and Non-Primitive Cells

In any point lattice a unit cell may be chosen in an infinite number of ways and may contain one or more lattice points per cell. It is important to note that unit cells do not "exist" as such in a lattice; they are a mental construct and can accordingly be chosen at ones convenience.

Any of the fourteen Bravais lattices may be referred to a primitive unit cell.

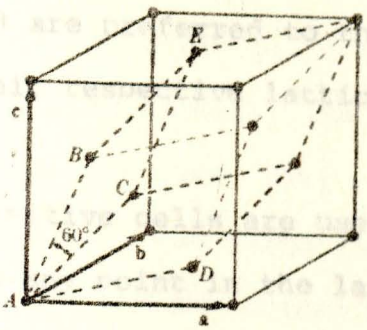


Fig.4 Face-centered cubic point lattice referred to cubic and rhombohedral cells.

For example, the face-centered cubic lattice shown in Fig.4 may be referred to the primitive cell indicated by the dashed lines. The lattice cell is rhombohedral; its axial angle α is 60°; and each of its axis is $1/\sqrt{2}$ times the length of the axes of the cubic cell. Each cubic cell has four lattice points associated with it each rhombohedral cell has one and the former has correspondingly four times the volume of the latter. Neverthless it is usually more convenient to use the cubic cell rather than the rhombohedral one because the former immediately suggests the cubic symmetry (which is higher than that of

the rhombohedral) which the lattice actually possesses. Similarly, the other centered non-primitive cell listed on Table 3 are preferred to the primitive cells possible in their respective lattices.

If non primitive cells are used the vector from the origion to any point in the lattice will now have components which are non integral multiples of the unit cell vectors. $\vec{a}$, $\vec{b}$, $\vec{c}$. The position of any lattice point in a cell may be given in terms of its co-ordinates; if the vector from the origin of the unit cell to the given point has components $u\vec{a}$, $v\vec{b}$, $w\vec{c}$ where u,v and w are fractions then the coordinates of the point are uvw. Thus, point A in Fig.4 taken as the origin, has coordinates 000 while point B, C and D, when referred to cubic axes, have coordinates 00½, ½ 0 ½ and ½½0 respectively.

4.1.5 Lattice Direction and Planes.

The direction of any line in a lattice may be described by first drawing a line through the origin parallel to the given line and then giving the coordinates of any point on the line through the origin. Let the line pass through the origin of the unit cell and any point having

coordinates xyz where this numbers are not necessarily integers. (This line also passes through the points 2x 2y 2z, 3x,3y,3z, etc). Then [xyz] written in square brackets, are the indices of the direction of the line. They are also indices of any line parallel to the given line, since the lattice is infinite and the origin may be taken at any point. Whatever the values of x,y,z, they are always converted to a set of smallest integers by multiplication or division throughout. Negative indices are written with a bar over the number.

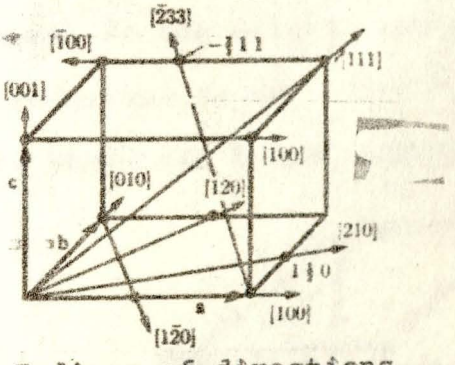


Fig.5 Indices of directions

The orientation of planes in a lattice may also be represented symbolically according to a system popularized by the English crystallographer Miller. A workable symbolism thus arrived at for the

orientation of a plane in a lattice, the Miller indices, which are defined as the reciprocals of the fractional intercepts which the plane makes with the cystallographic axes. For example, if the Miller indices of a plane are (hkl) written in paranthesis, then the plane makes fractional intercepts of $1/_h$, $1/_k$, $1/_\ell$ with the axes, and if the axial lengths are a,b,c, the plane makes actual intercepts of $a/_h$, $a/_k$, $c/_\ell$, as shown in Fig.6. Parallel to any plane in any lattice, there is a whole set of parallel equidistant planes, one of which passes through the origin; the Miller indices (hkℓ) usually refer to that plane in the set which is nearest to the origin, although they may be taken as referring to any other plane in the set or to the whole set taken together. If a plane

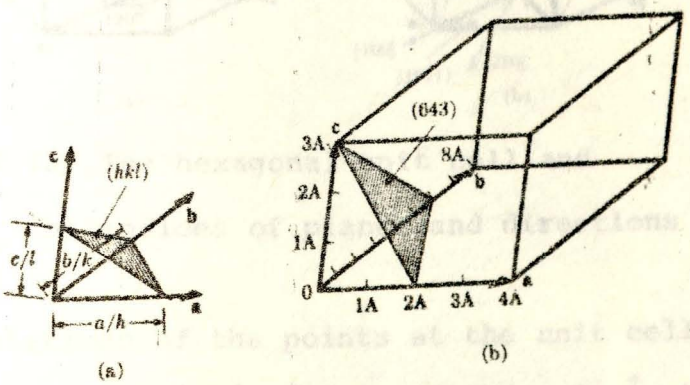


Fig.6 Plane designation by Miller indices

cuts a negative axes the corresponding index is negative and is written with a bar over it. The planes (nh nk nℓ) are parallel to the plane (hkℓ) and have 1/n the spacing.

A slightly different system of plane indexing is used in the hexagonal system. The unit cell of a hexagonal lattice is defined by two equal and co-planar vector $\vec{a}_1$ and $\vec{a}_2$ at 120° to one another and a third axis $\vec{c}$ at right angles (Fig.7). The complete lattice is built up, as usual by repeated

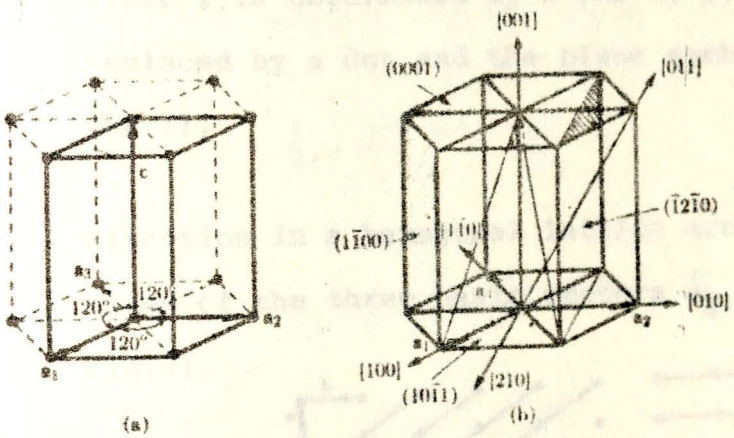


Fig.7 (a) The hexagonal unit cell and
(b) indices of planes and directions

translations of the points at the unit cell corners by the vector $\vec{a}_1$ $\vec{a}_2$ $\vec{c}$. The third axis $\vec{a}_3$ lying in

the basal plane of a hexagonal prism, is so symmetrically related to $\vec{a}_1$ and $\vec{a}_2$ that is often used in conjunction with the other two. Thus, the indices of a plane in the hexagonal system, called Miller-Baravais indices, refer to four axes and are written (hkiℓ). The index i is the reciprocal of the fractional intercept on the a_3 axis.

$$\begin{aligned} \vec{a}_1 + \vec{a}_2 &= - \vec{a}_3 \quad \text{then} \\ h + k &= - i \end{aligned} \tag{2}$$

Since i is determined by h and k, it is sometimes replaced by a dot and the plane symbol is written (hk.ℓ).

Direction in a hexagonal lattice are expressed in terms of the three basic vectors $\vec{a}_1$, $\vec{a}_2$ and $\vec{c}$ (see Fig.7).

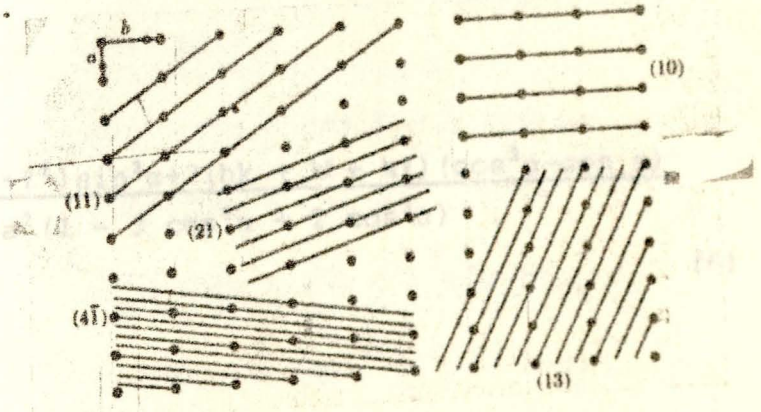


Fig.8 Two-dimensional lattice, showing that lines of lowest indices have the greatest spacing and the greatest density of lattice points.

The various sets of planes in a lattice have various values of interplanar spacings. The planes of large spacing have low indices and pass through a high density of lattice points, where as the reverse is true for of planes of small spacings (see Fig.8). The interplaner spacing $d_{hk\ell}$ measured at right angle to the planes, is a function both of the plane indices ($hk\ell$) and the lattice constant ($a, b, c, \alpha, \beta, \gamma$). The exact relation depends on the crystalssystem involved and for the cubic system takes on the relatively simple form.

$$\text{Cubic} \quad d_{hk\ell} = \frac{a}{\sqrt{h^2+k^2+\ell^2}} \tag{3}$$

Interplanar spacing equation for the other systems are:

$$\text{Tetragonal:} \quad \frac{1}{d^2} = \frac{h^2+k^2}{a^2} + \frac{\ell^2}{c^2} \tag{4}$$

$$\text{Hexagonal:} \quad \frac{1}{d^2} = \frac{4}{3}\left(\frac{h^2+hk+k^2}{a^2}\right) + \frac{\ell^2}{c^2} \tag{5}$$

Rhombohedral:

$$\frac{1}{d^2} = \frac{(h^2+k^2+\ell^2)\sin^2\alpha + 2(hk+k\ell+h\ell)(\cos^2\alpha-\cos\alpha)}{a^2(1-3\cos^2\alpha+2\cos^3\alpha)} \tag{6}$$

Orthorhombic:

$$\frac{1}{d^2} = \frac{h^2}{a^2} + \frac{k^2}{b^2} + \frac{\ell^2}{c^2} \qquad (7)$$

Monoclinic:

$$\frac{1}{d^2} = \frac{1}{\sin^2\beta}\left(\frac{h}{a^2} + \frac{k^2\sin^2\beta}{b^2} + \frac{\ell^2}{c^2} - \frac{2h\ell\cos\beta}{ac}\right) \qquad (8)$$

and

Triclinic:

$$\frac{1}{d^2} = \frac{1}{V^2}(S_{11}h^2+S_{22}k^2+S_{33}\ell^2+2S_{12}hk+2S_{23}k\ell+2S_{13}h\ell), \qquad (9)$$

where, in the equation for triclinc crystals

V = volume of unit cell

$S_{11} = b^2c^2 \sin^2\alpha$

$S_{22} = a^2c^2 \sin^2\beta$

$S_{33} = a^2b^2 \sin^2\gamma$

$S_{12} = abc^2 (\cos\alpha \cos\beta - \cos\gamma)$,

$S_{23} = a^2bc (\cos\beta \cos\gamma - \cos\alpha)$,

$S_{13} = ab^2c (\cos\gamma \cos\alpha - \cos\beta)$.

4.2. The Intensities of Diffracted Beams

The resultant wave scattered in a certain direction by all the atoms of the unit cell is called the geometrical structure factor and is designated by the symbol F. It is obtained by simply adding together all the waves scattered by the individual atoms. If a unit cell contains atoms 1,2,3,.....,N, with fractional coordinates, given in terms of the magnitude of the crystal axes $u_1v_1w_1$, $u_2v_2w_2$,.....$u_Nv_Nw_N$ and atomic scattering factor (the resultant wave scattered in a certain direction by all the electrons present in an atom)

f_1, f_2,....., f_N, then the structure factor for the hkℓ reflection is given by

$$F_{hkl} = \sum^{N} f_n \exp 2\pi i\,(hu_n + kv_n + \ell w_n) \qquad (10)$$

Since F is in general a complex number, it expresses both the amplitude and the phase of the resultant wave. Its absolute value |F| gives the amplitude of the resultant wave in terms of the amplitude of the wave scattered by a single electron.

The intensity of the beam diffracted by all the atoms of the unit cell in a direction predicted by the Bragg's Law is simply proportional to $|F|^2$, the square of the amplitudes of the resultant beam.

Since F depends on the Miller indices and the coordinates of the atoms in the unit cell, (as seen from Eq. (10)) there will be certain reflections which are absent even though Bragg's Law is satisfied. The conditions for general reflections hkl to be present or absent are given in Table 4.

Table 4. Condition for reflection and extinction for different lattice types

Lattice type	Reflection present	Reflection absent
simple	all	non
base-centred	h and k unmixed (one even and other odd)	h and k mixed
body-centred	(h+k+l) even	(h+k+l) odd
face-centred	h, k and l unmixed all odd or all even	h, k and l mixed

4.3. Determination of Crystal Structure /23/.

The basic principle involved in structure determination is based on the following: The crystal structure of a substance determines the diffraction pattern of that substance, ie. the shape and size of the unit cell

determines the angular position of the diffracted lines and the arrangement of the atoms within the unit cell determines the relative intensities of the lines. In view of the above, in an indirect manner, the structure is determined from the diffraction pattern.

The determination of an unknown structure proceeds in three major steps:

1. The shape and the size of t unit cell are deduced from the angular position of the diffraction lines. An assumption is first made as to which of the crystal systems the unknown structure belongs to, and then on the basis of this assumption the correct Miller indices are assigned to each reflection. This step is called 'indexing of pattern' and is only possible when the correct choice of crystal system has been made. Once this is done, the shape of the unit cell is known (from the crystal system), and its size is calculable from the position of the Miller indices of the diffraction lines.

2. The number of the atoms per unit cell is then computed from the shape and size of the unit cell, the chemical composition of the specimen and its measured density.

3. Finally, the position of the atoms within the unit cell are deduced from the relative intensities of the diffraction lines.

Only when these three steps have been accomplished is the structure completely determined. The third step is generally the most difficult. Nevertheless the shape and the size of the unit cell, without any knowledge of atom positions, is in itself of very great value in many applications. The procedures given below for indexing patterns are applicable whether the structure is known or not but they are of course very much easier to apply if the structure is known before hand.

For this work it suffices to mention the procedures for indexing cubic, tetragonal and hexagonal systems by the graphical method.

4.3.1 Indexing Pattern of Cubic Crystals /23/.

The interplanar spacing equation for a cubic system is

$$d_{hkl} = (h^2 + k^2 + l^2)^{-\frac{1}{2}} a \qquad (11)$$

Now the sum of the three integers squared can only have the values 1,2,3,4,5,6,8,9, ... or in otherwords, all integer values except $4^p(8n + 7)$, where p and n can have all integer values, including zero.

This means that the above equation (Eq. 11) predicts the same set of d values for all cubic crystals, except for a scale factor, namely, the cell edge a. It is simple and convenient, therefore to construct a graph on which the above relation is plotted for each possible combination of h, k and l. Such a graph is shown in Fig. 1. To use it, the observed d values are marked on a strip of paper using the scale of the bottom of the graph and, keeping d = 0 on the ordinate, the strip is placed horizontally across the appropriate a value (structure is known beforehand and referred from earlier work). The hkl values of each reflection are then read off directly. This procedure can also be used with equal ease when the magnitude of the lattice constant a is not known before hand.

Since d = 0 is fixed to lie along the ordinate, and since the scale along which d is measured must remain parallel to the abscissa, a paper strip on which the d values have been plotted is moved upward until a match

between the lines on the graph and the marks on the paper strip are obtained. The unknown value of a then can be read on the ordinate, and the indices can be assigned to each reflection as before.

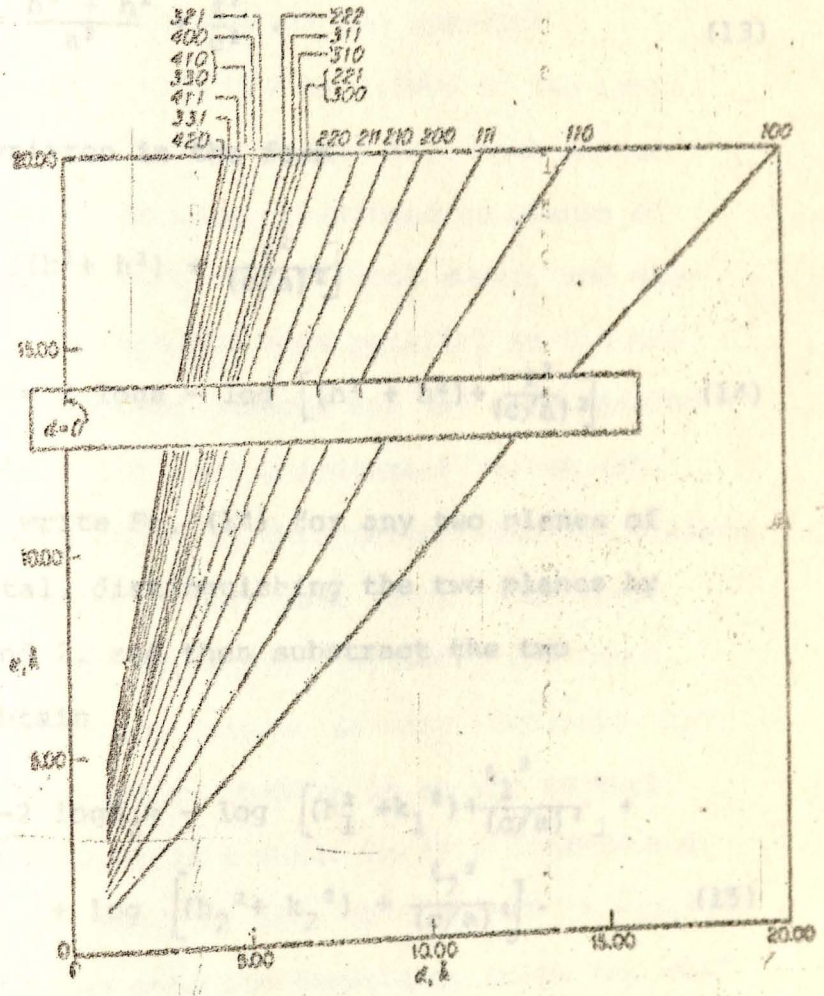


Fig.9. Plot of $d_{hkl} = (h^2 + k^2 + l^2)^{-\frac{1}{2}}a$ for each possible combination of h, k, and l.

4.3.2 Indexing Pattern of Tetragonal Crystals (Graphical Methods) /24/

The plane-spacing equation for the tetragonal system involves two unknown parameters, a and c:

$$\frac{1}{d^2} = \frac{h^2 + h^2}{a^2} + \frac{\ell^2}{c^2} . \qquad (13)$$

This may be rewritten in the form

$$\frac{1}{d^2} = \frac{1}{a^2}\left[(h^2 + h^2) + \frac{\ell^2}{(c/a)^2}\right]$$

$$2 \log d = 2 \log a - \log \left[(h^2 + h^2) + \frac{\ell^2}{(c/a)^2}\right] \qquad (14)$$

suppose we now write Eq. (14) for any two planes of tetragonal crystal, distinguishing the two planes by subscripits 1 and 2, and then substract the two equations. We obtain

$$2 \log d_1 - 2 \log d_2 = - \log \left[(h_1^2 + k_1^2) + \frac{\ell_1^2}{(c/a)^2}\right] + \log \left[(h_2^2 + k_2^2) + \frac{\ell_2^2}{(c/a)^2}\right] . \qquad (15)$$

This equations shows that the difference between the 2 logd values for any two planes is independent of a and

depends only on the axial ratio c/a and the indices hkl of each plane. This fact was used by Hull and Davey as the basis for a graphical method of indexing the powder patterns of tetragonal crystals.

The construction of Hull-Davey chart is illustrated in Fig.10. First, the variation of the quantity $((h^2+ k^2) + l^2/(c/a)^2)$ with c/a is plotted on two-range semilog paper for particular values hkℓ. Each set of indices hkℓ, as long as they corrospond to planes of different spacing, produce a different curve, and when $\ell = 0$ the curve is straight line parallel to the c/a axis. Planes of different indices but the same spacing such as (100) and (010), are represented by the same curve on the chart, which is then marked with the indices of either one of them in this case (100). (The chart shown is for a simple tetragonal lattices, one for a body-centered tetragonal lattice is made simple by omitting all curves for which $(h+k+\ell)$ is an odd number). A single-range logarithmic d scale is then constructed it extends over two range of the $(h^2+ k^2)+l^2\ \ell^2/(c/a^2)$ scale and runs in the opposite direction, since the coefficient of ~~log~~d in Eq. (14) is -2 times the coefficient of log $(h^2+ k^2) + \ell^2/(c/a)^2$. This means that the d

values of two planes for a given c/a ratio, are separated by the same distance on the scale as

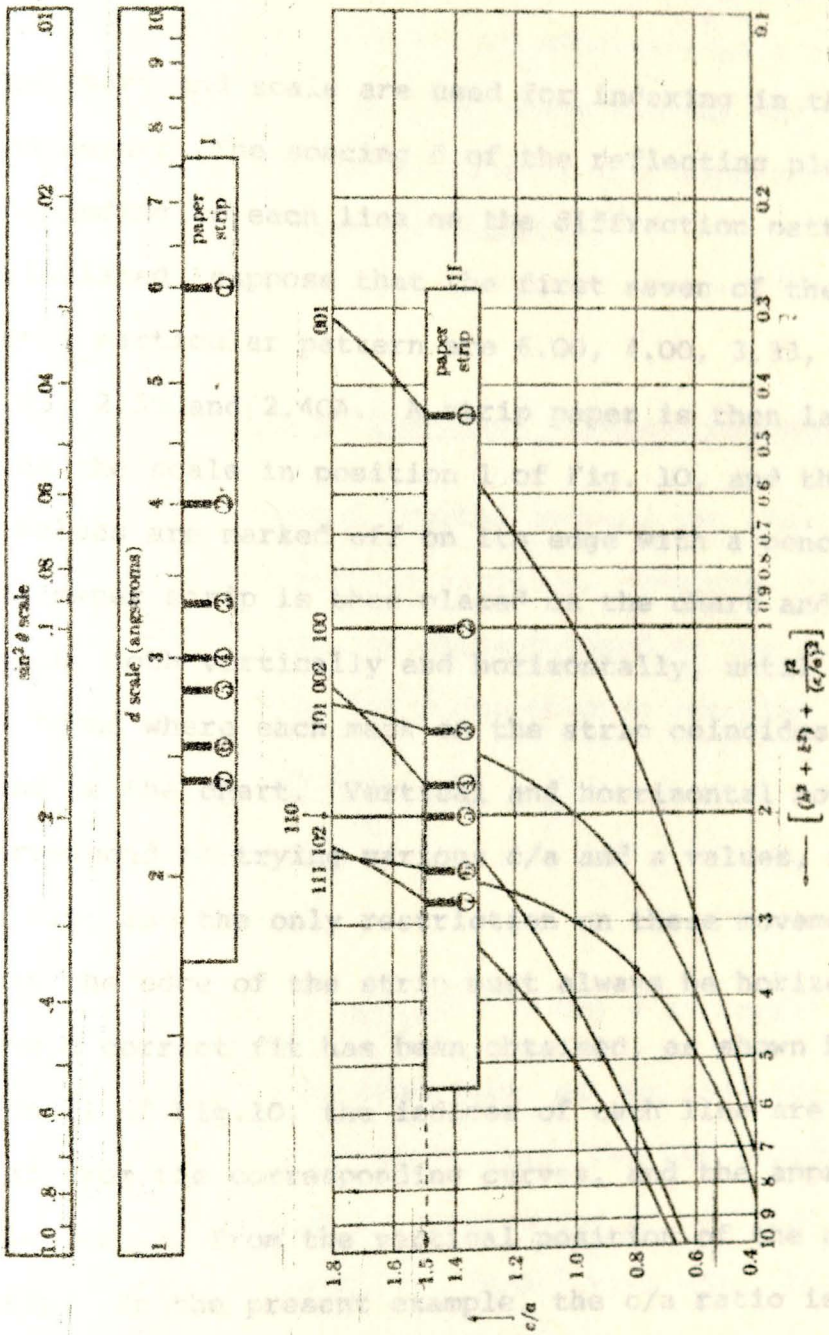


Fig.10 Partial Hull-Davey chart for a simple tetragonal system.

the horizontal separation, at the same c/a ratio, of the two corresponding curves on the chart.

The chart and scale are used for indexing in the following manner. The spacing d of the reflecting planes corresponding to each line on the diffraction pattern is calculated, suppose that the first seven of these values for a particular pattern are 6.00, 4.00, 3.33, 3.00, 2.83, 2.55 and 2.40A. A strip paper is then laid alongside the scale in position 1 of Fig. 10, and the observed d values are marked off on its edge with a pencil. The The paper strip is then placed on the chart and moved about, both vertically and horizontally, until a position is found where each mark on the strip coincides with a line on the chart. Vertical and horrizontal movements correspond to trying various c/a and a values, respectively, and the only restriction on these movements is that the edge of the strip must always be horizontal. When a correct fit has been obtained, as shown by position 11 of Fig.10, the indices of each line are simply read from the corresponding curves, and the approximate value of c/a from the vertical position of the paper strip. In the present example, the c/a ratio is 1.5 and the first line on the pattern (formed by planes of spacing 6.00A) is a 001 line, the second a 100 line, the third a 101 line etc. After all the line have been indexed

in this way, the d values of the two highest-angle lines are used to set up two equations of the form of Eq.(13), and these are solved simultaneously to yield the values of a and c. From these values, the axial ratio c/a may then be calculated with more precision than it can be found graphically.

4.3.3 Indexing Pattern of Hexagonal Crystals (Graphical Method) /24/

Patterns of hexagonal crystal systems can also be indexed by graphical methods since the hexagonal unit cell like the tetragonal, is characterised by two variable parameters a and c. The plane-spacing equation is:

$$d^{-2} = \frac{4}{3}\ \frac{h^2 + hk + k^2}{a^2} + \frac{\ell^2}{c^2} \qquad (16)$$

or

$$2 \log d = 2 \log a - \log\left[\frac{4}{3}(h^2+k^2+ hk) + \ell^2/(c/a)^2\right] \qquad (17)$$

which is exactly the same form as Eq. (14) for the tetragonal system . A Hull-Davey chart for the hexagonal system can therefore be constructed by plotting the variation of $\log \frac{4}{3}(h^2+hk+k^2)+\ell^2/(c/a)^2$ with c/a. Special charts for hexagonal close-packed lattices may also be prepared by omitting all curves for which (h+2k) is an integral multiple of b and ℓ is odd.

Indexing and the determination of the c/a ratio, here, is done in a similar way as that for the tetragonal system. Fig.11 is a Hull-Davey chart along with the d scale for the hexagonal system.

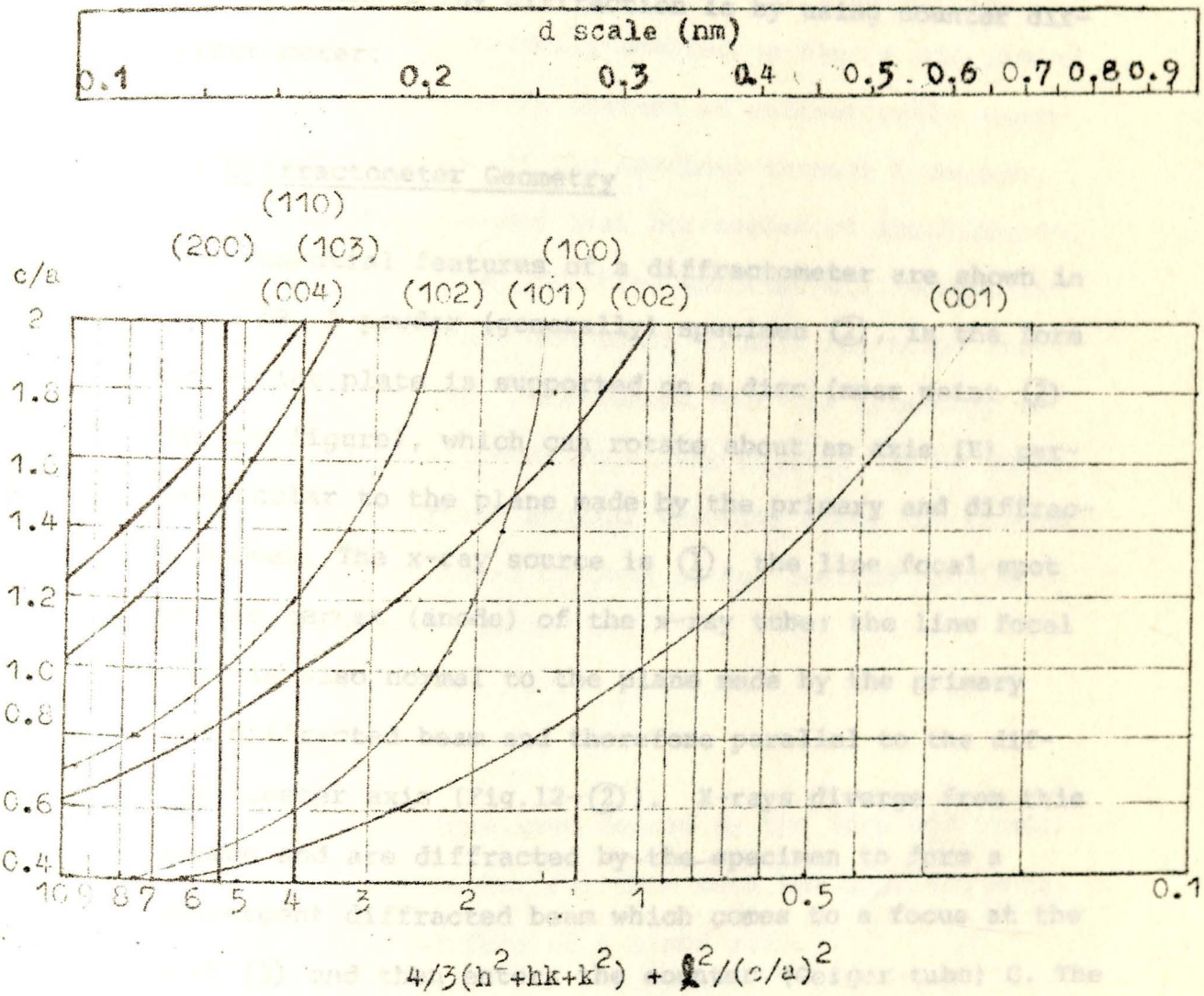


Fig.11 Hull-Davey chart for hexagonal crystals (partial)

4.4 X-Ray Diffraction

4.4.1 Counter Diffractometer

The most efficient and accurate way of measuring and interpreting x-ray diffraction is by using counter diffractometer.

4.4.1.1 Diffractometer Geometry

The essential features of a diffractometer are shown in Fig. 12. A powder (generally) specimen (2), in the form of a flat plate is supported on a disc (near point (2) in the figure), which can rotate about an axis (E) perpendicular to the plane made by the primary and diffracted beam. The x-ray source is (1), the line focal spot on the target (anode) of the x-ray tube; the line focal spot is also normal to the plane made by the primary and diffracted beam and therefore parallel to the diffractometer axis (Fig.12-(2)). X-rays diverge from this source and are diffracted by the specimen to form a convergent diffracted beam which comes to a focus at the slit (3) and then enters the counter (Geiger tube) G. The receiving parallel slit assembly and divergence parallel slit assembly are special slits which define and collimate the incident and diffracted beams.

The receiving slits and counters are supported on a carriage which may be rotated about the diffractometer axis and whose angular position 2 θ may be read on a graduated scale placed along the diffractometer circle. The support of the receiving slit (or counter) and specimen are mechanically coupled so that a rotation of the counter through 2X degrees is automatically accompanied by rotation of the specimen through X degrees. This coupling insures that the angles of incidence on, and reflection from, the flat specimen will always be equal to one another and equal to half the total angle of diffraction, an arrangement which is necessary to preserve focusing conditions. The counter may be power-driven at a constant angular velocity about the diffractometer axis or moved by hand to any desired angular position.

4.4.1.2 Specimen

The kind of specimen used depend on the form and amount of material available. For this work the specimen were adhered to the surface of a glass slide.

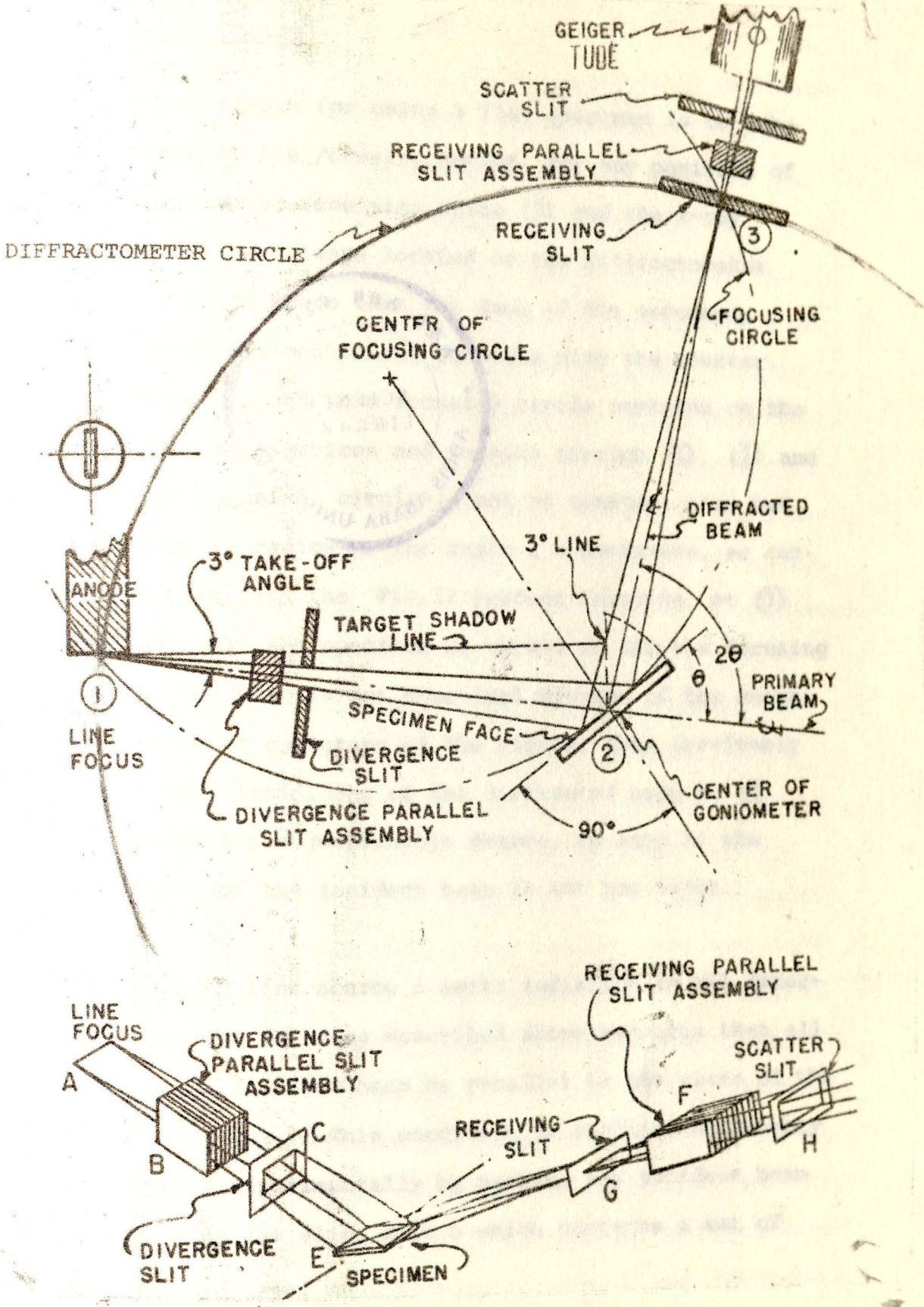


Fig.12 Basic focusing geometry of the used diffractometer

4.4.1.3 X-ray Optics

The chief reason for using a flat specimen is to take advantage of the focusing action. For any position of the counter the receiving slits (3) and the x-ray source (1) are always located on the diffractometer circle, which means that the face of the specimen, because of its mechanical coupling with the counter, is always tangent to a focusing circle centered on the normal to the specimen and passing through (1), (2) and (3). The focusing circle is not of constant size but increases in radius as the angle 2 θ decreases, as can be inferred from the Fig.12.Perfect focusing at (3) requires that the specimen be curved to fit the focusing circle, but that is not practical because of the changing radius of curvature of the circle. This inevitably causes some broadining of the diffracted beam at (3) but not to any objectionable degree, so long as the divergence of the incident beam is not too large.

The extended line source A emits radiation in all direction, but the focusing described above requires that all rays in the incident beam be parallel to the plane of the upper drawing (Fig.12).This condition is realized as closely as possible experimentally by passing the incident beam through a Soller slit, slit B which contains a set of

closely spaced, thin metal plates parallel to the plane of the diffractometer circle. These plates remove a large proportion of rays inclined to the plane of the diffractometer circle and still allow the use of a line source of considerable length. Typical dimensions of Soller slit are: length of plates 32 mm, thickness of plates 0.05 mm, clear distance between plates 0.43 mm. At either end of the slit assembly are rectangular slits G and H for slit assembly F and C for slit assembly B. The combination of slits and plates breaks up the incident beam into a set of triangular wedges of radiation. There are, of course, some rays, not shown in the drawing, which diverge in planes perpendicular to the plane of plates (of the Soller slit), and these rays cause the wedges of radiation to merge into one another a short distance away from the divergence slit. However, the long, closely spaced plates do restrict this unwanted divergence to an angle of about 1.5°. The slits commonly available have divergence angles ranging from very small values upto about 4° . In the forward reflection region, a divergence angle of 1° is sufficient because of the low inclination of the specimen surface to the incident beam, but in the back reflection an increase in the divergence angles to 3 or 4° will increase the diffracted intensity. But if line intensities are to be compared over the whole range of 2 θ, the same divergence must be used throughout

and the specimen must be wider than the beam at all angles.

The beam diffracted by the specimen passes through another Soller slit assembly and a receiving slit (3) before entering the counter. Since the receiving slit defines the width of the beam admitted to the counter, an increase in its width will increase the maximum intensity of any diffraction line being measured but at the expense of some loss of resolution.

Because of the focusing of the diffracted rays and the relatively large radius of the diffractometer circle, about 15 cm in commercial instruments, a diffractometer can resolve very closely spaced diffraction lines. Such high resolution can only be achieved with a correctly adjusted instrument, and it is necessary to so align the component parts that the following conditions are satisfied for all diffraction angles.

1. Line source, specimen surface, and divergence slit are all parallel,
2. the specimen surface coincides with the diffractometer axis, and
3. the line source and receiving slit both lie on the diffractometer circle.

4.4.1.4 Recording Diffracted Radiation

The intensity of the diffracted beam is measured directly in terms of the rate at which the diffracted photons trigger the counting device. The counting device, which may be the Geiger, the proportional or the scintillation type, depends on the ionization produced by the incident photons and scans the circumference of the circle which would have carried the photographic film in a powder camera. A proportional or scintillation counter used to record the x-ray intensities has the advantage that the pulse-height analyser can be adjusted to eliminate most of the white radiation although at the same time it allows through a large proportion of the higher intensity characteristic radiation.

5. EXPERIMENTAL PROCEDURE

5.1 Apparatus Used for X-ray Diffraction

X-ray for diffraction work is produced by bombarding a suitable metallic surface with electrons which have

been accelerated toward the target under a potential difference which may lie between 20 and 90 kV.

XRG 300 X-ray Generator (Philips) was used with a copper-target tube, so that the wavelength for the investigations was the CuK - radiation (= 0.154 nm). The CuK - radiation is filtered out by means of a Ni-filter, the white radiation is filtered out by means of the pulse-height analyser of the detector circuit. A Norelco Wide Range Diffractometer (Type 150,100.00) was used for the structure analysis of the thin-film solar cell materials.

5.2 Preparation of Thin Films

5.2.1 CdS Films

CdS films were prepared by screen printing and sintering (3.1.3), by evaporation (3.1.1), and by conversion of CdO to CdS (3.1.6).

CdS paste for screen printing was prepared by mixing 1 g CdS powder and 0.1 g $CdCl_2$ powder with propane 1-2 diol (binder) in an agate mortar. The $CdCl_2$ was used as a flux. The CdS paste was printed on a clean or SnO_2 - coated glass substrate by a screen printing method, and then sintered at a temperature of 600 - 650°C in a vacuum of 80 - 100 Pa for 30 minutes using a furnace, shown in Fig.13.

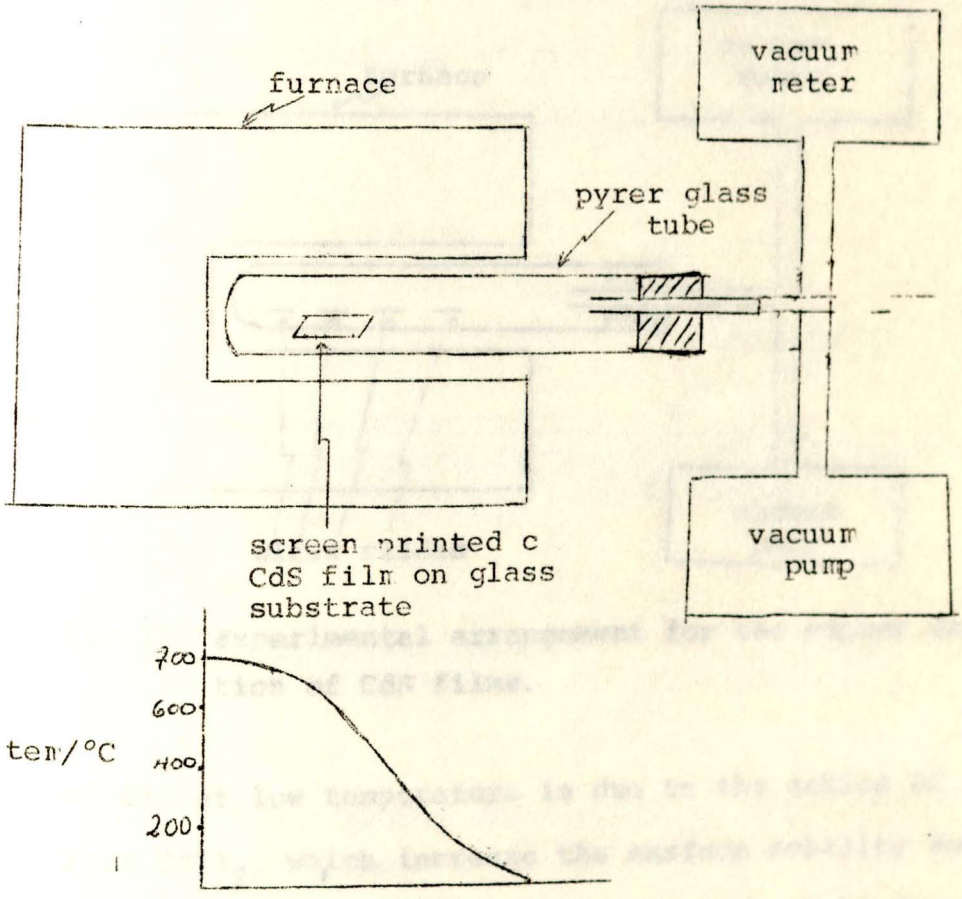


Fig.13. Experimental arrangement of the furnace used for sintering and its temperature profile.

The temperature profile of the furnace was measured by a Cu/Fe thermocouple.

During the sintering of the screen printed CdS films a CdS deposition on the glass tube was observed. By placing glass slide (as substrate) in the glass tube, vapour deposited CdS films for different substrate temperatures were obtained. The reason for the evaporation

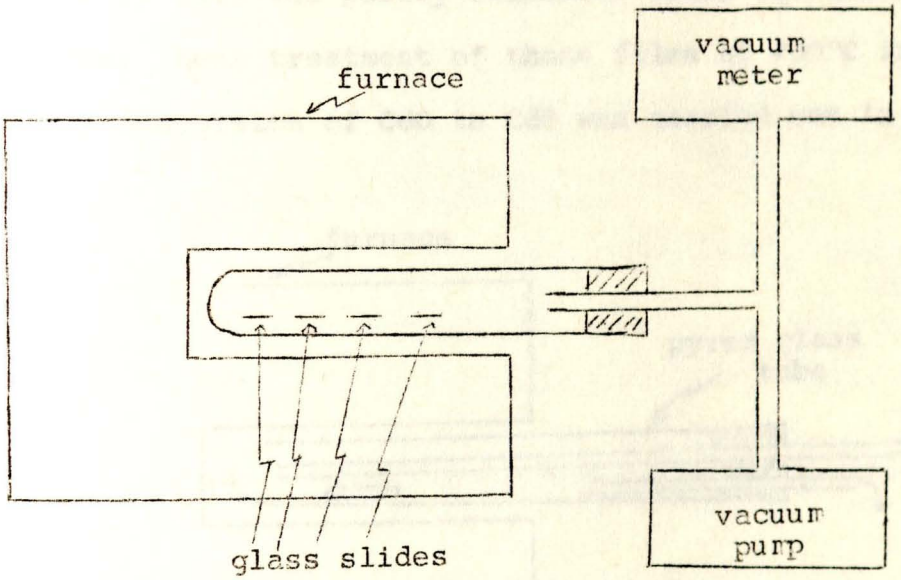


Fig.14. Experimental arrangement for the vapour deposition of CdS films.

of CdS at low temperature is due to the action of the flux $CdCl_2$, which increase the surface mobility and therefore, the evaporation rate of CdS. A bigger amount of CdS paste prepared as for screen printing was used to increase the thickness of the deposited films.

It is also found, that with increase of the percentage of $CdCl_2$ in the $CdS/CdCl_2$ mixture the amount of evaporated CdS increases.

For conversion of CdO films to CdS, Cd films were deposited by evaporation of pure Cd onto a glass substrate in an apparatus similar to that used for sintering and evaporation of CdS.(see Fig.14). During the deposition the Cd film was partly oxidized. Total oxidation ocurred after heat treatment of these films at 400°C in air. The conversion of CdO to CdS was carried out in the tube

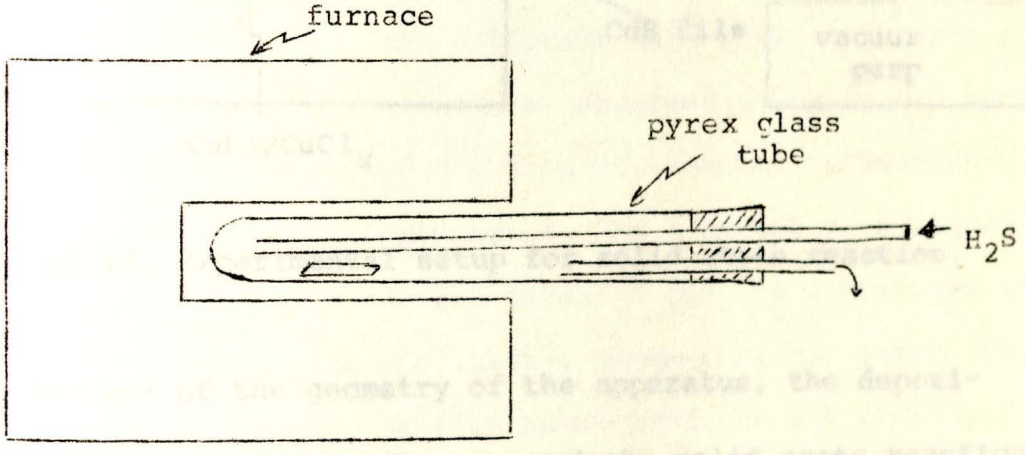


Fig.15. Experimental arrangement for sulphidation of CdO films.

inserted in the furnace (Fig.15) at a temperature of about 450°C, with flowing H_2S from a Kipp's apparatus

in which reaction between FeS_2 and HCl is going on.

5.2.2 Cu_xS Flims

Cu_xS layers were prepared by solid state reaction of screenprinted CdS films with evaporated CuCl / $CuCl_2$ mixture film in vacuum (see 3.2.4., Fig.16).

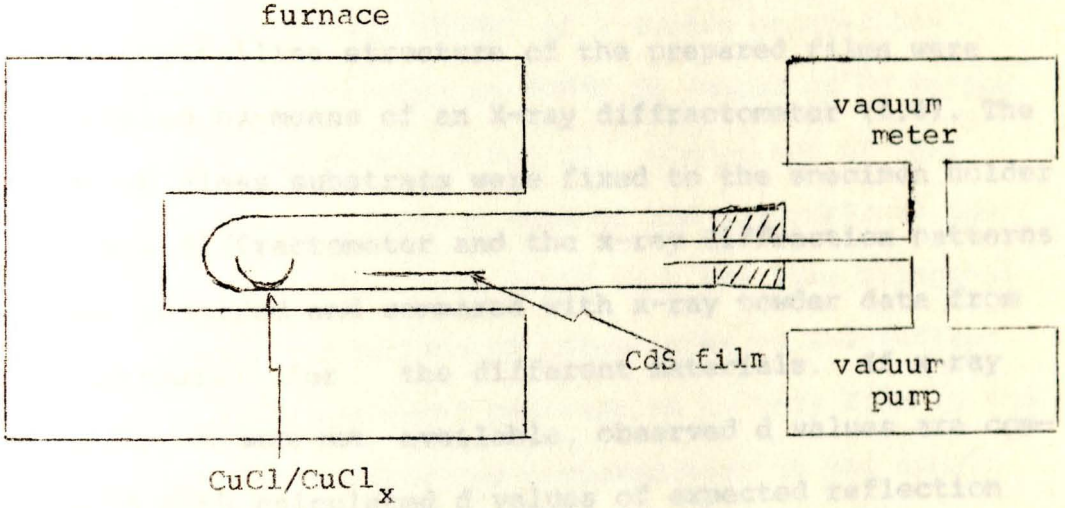


Fig.16. Experimental setup for solid state reaction.

Because of the geometry of the apparatus, the deposition of CuCl/$CuCl_2$ mixture and the solid state reaction between CuCl/$CuCl_2$ mixture and CdS was taking place simultaneously, when the CdS film was placed where the temperature in the glass tube was around 500°C.

5.2.3 SnO_2 Films

SnO_2 layer was prepared by chemical vapour deposition of $SnCl_2$ in air on a glass slide kept at a temperature greater than 450°C.

5.3 Analysis of the Structure of Thin Films Prepared.

The crystalline structure of the prepared films were analysed by means of an X-ray diffractometer (4.4). The coated glass substrats were fixed to the specimen holder of the diffractometer and the x-ray diffraction patterns were recorded and compared with x-ray powder data from literature for the different materials. If x-ray powder data were not available, observed d values are compared with calculated d values of expected reflection once the system is determined. The d values of expected reflections for a certain material can be calculated if its crystal system and lattics parameters are known. The crystal system and lattice parameters for the different materials are referred from literature whenever possible.

5.4 Experimental Results and Discussion.

5.4.1 CdS Films

5.4.1.1 Screen-Printed Films.

Table 5 shows the x-ray powder data for CdS. An x-ray diffraction pattern (XRDP) of a screen-printed CdS layer, after sintering at 640°C in vacuum of 80 Pa for 20 minutes, is shown in Fig.17. Comparison of this pattern with diffraction data of the (polycrystalline) CdS-powder, the film was found with the same hexagonal structure. A comparison of intensities of the reflections shows a preferred orientation of this film in the (010) and (110) direction perpendicular to the substrate surface.

Since Matsumoto et al /10/ have not analysed the crystalline structure of their screen-printed and sintered films, comparison interms of structure and preparation condition of their film with the one prepared here, was not possible.

Table 5. X-ray powder data for cadmium sulphide /25/

CdS.

Hexagonal a = 4,132 Å = 6,737 Å

Relative intensity	Θ (CuKα)	d/Å	hkℓ
8	12.4	3.58	010
7	13.25	3.37	002
10	14.05	3.16	011
3	18.35	2.45	012
7	21.85	2.07	110
6	23.95	1.90	013
1	25.5	1.79	020
5	26	1.76	112
2	26.5	1.73	021
½	27.35	1.68	004
1	29.2	1.58	022
½	30.4	1.52	014
4	33.45	1.40	023
1	34.75	1.35	120
4	35.5	1.33	121
½	36.35	1.31	124

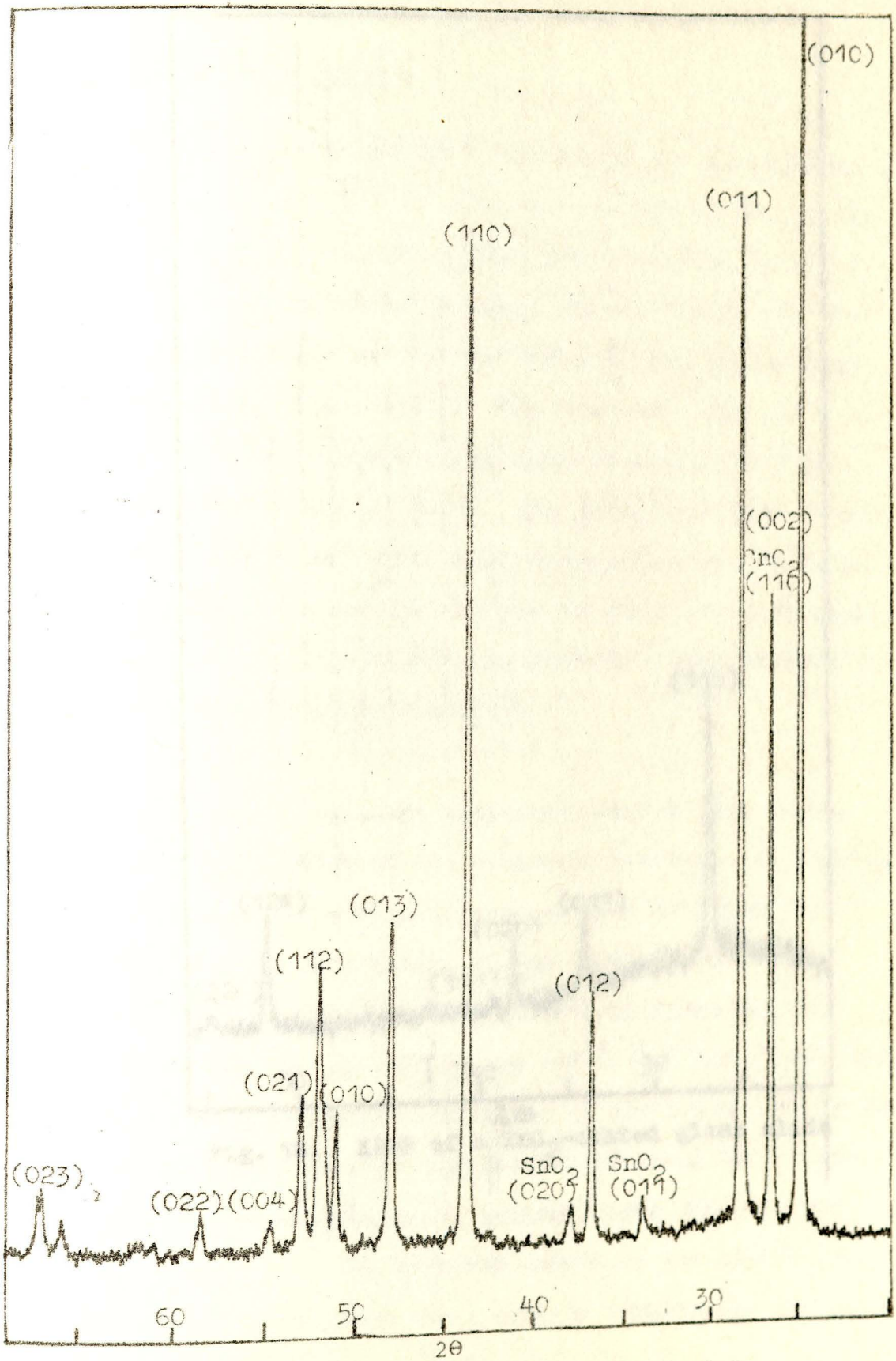


Fig.17. XRDP of a screen-printed CdS film on SnO_2 coated glass slide.

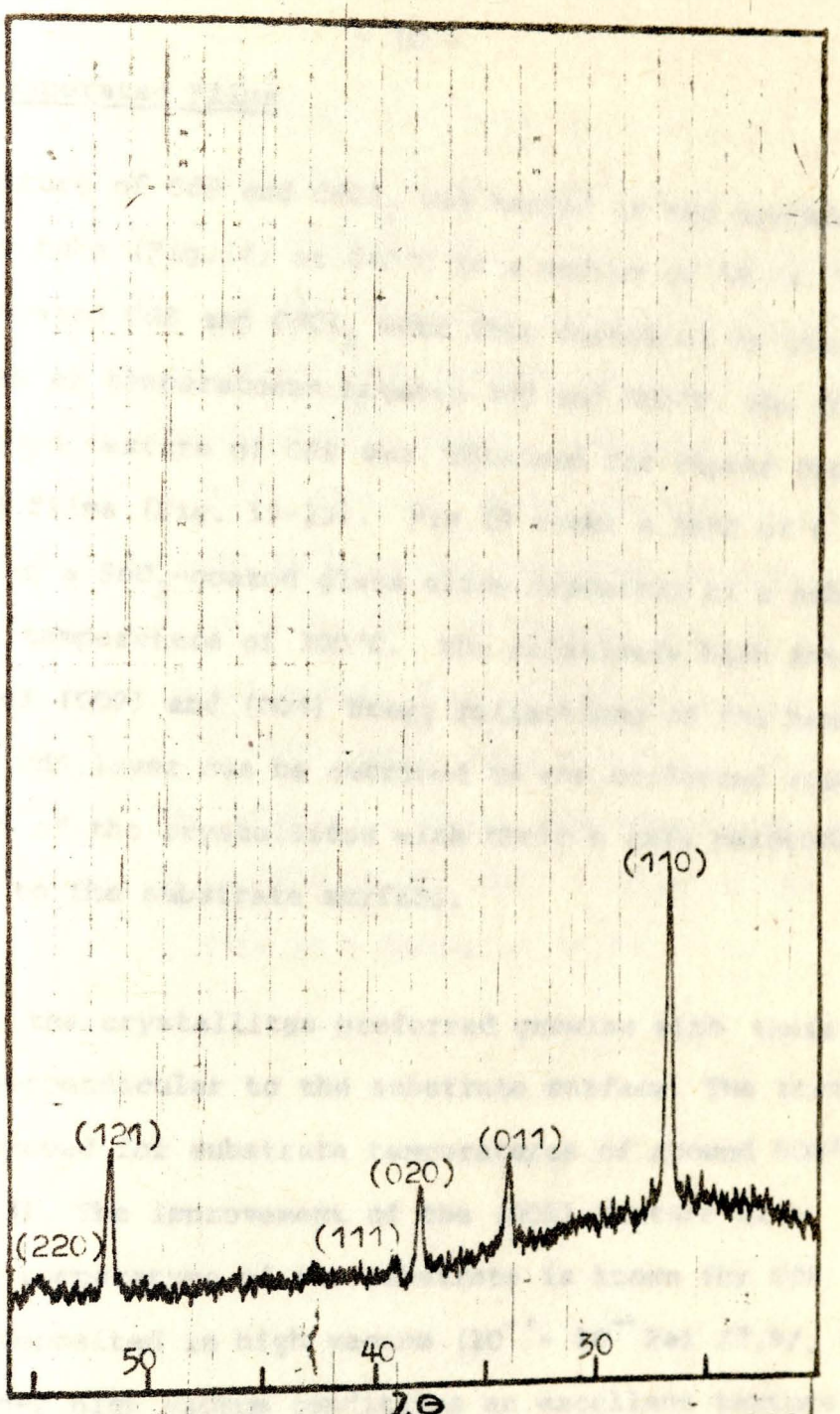


Fig. 18. XRDP of a SnO_2-coated glass slide

5.4.1.2 Evaporated Films

A mixture of CdS and $CdCl_2$ was heated in the horizontal glass tube (Fig.14) at 640°C in a vacuum of 80 Pa. The evaporated CdS and $CdCl_2$ were then deposited on glass slides at temperatures between 300 and 500°C. The (001) oriented texture of CdS was obtained for vapour deposited films (Fig. 19-23). Fig.19 shows a XRDP of a CdS film on a SnO_2-coated glass slide deposited at a substrate temperature of 300°C. The relatively high intensity of (002) and (004) Bragg reflections of the hexagonal CdS layer can be ascribed to the preferred orientation of the crystallites with their c axis perpendicular to the substrate surface.

Hence, the crystallites preferred growing with their axis perpendicular to the substrate surface. The texture is improved for substrate temperatures of around 500°C (Fig.23). The improvement of the (001) texture with higher temperature of the substrate is known for CdS films deposited in high vacuum (10^{-3} - 10^{-4} Pa) /7,9/, too. But under high vacuum conditions an excellent texture is possible for substrate temperature of about 200°C. Under the low vacuum conditions, attained here (80 Pa), the influence on the textured growth by the higher air pressure in the glass tube, must be compensated for by a

higher mobility of deposited atoms and rolecules This higher mobility of the atoms or molecules increases with increase in substrate temperature. If the percentage of $CdCl_2$ - in the evaporated mixture is around 50%, then it is found, that reflections of $CdCl_2$ in the XRDP of the deposited film appear for substrate temperature < 400°C (Fig.20). These reflections are found to disappear after a heat treatment at about a temperature of 500°C for 10 - 20 minutes (Fig.21 and 22), nevertheless, there appear other reflections which spoil the texture of the CdS layers. This underlines that a heat treatment of the $CdS/CdCl_2$ vapor deposited layer does not improve the quality of the (001) texture of the CdS layer, if it is done in a vacuum of 80 Pa.

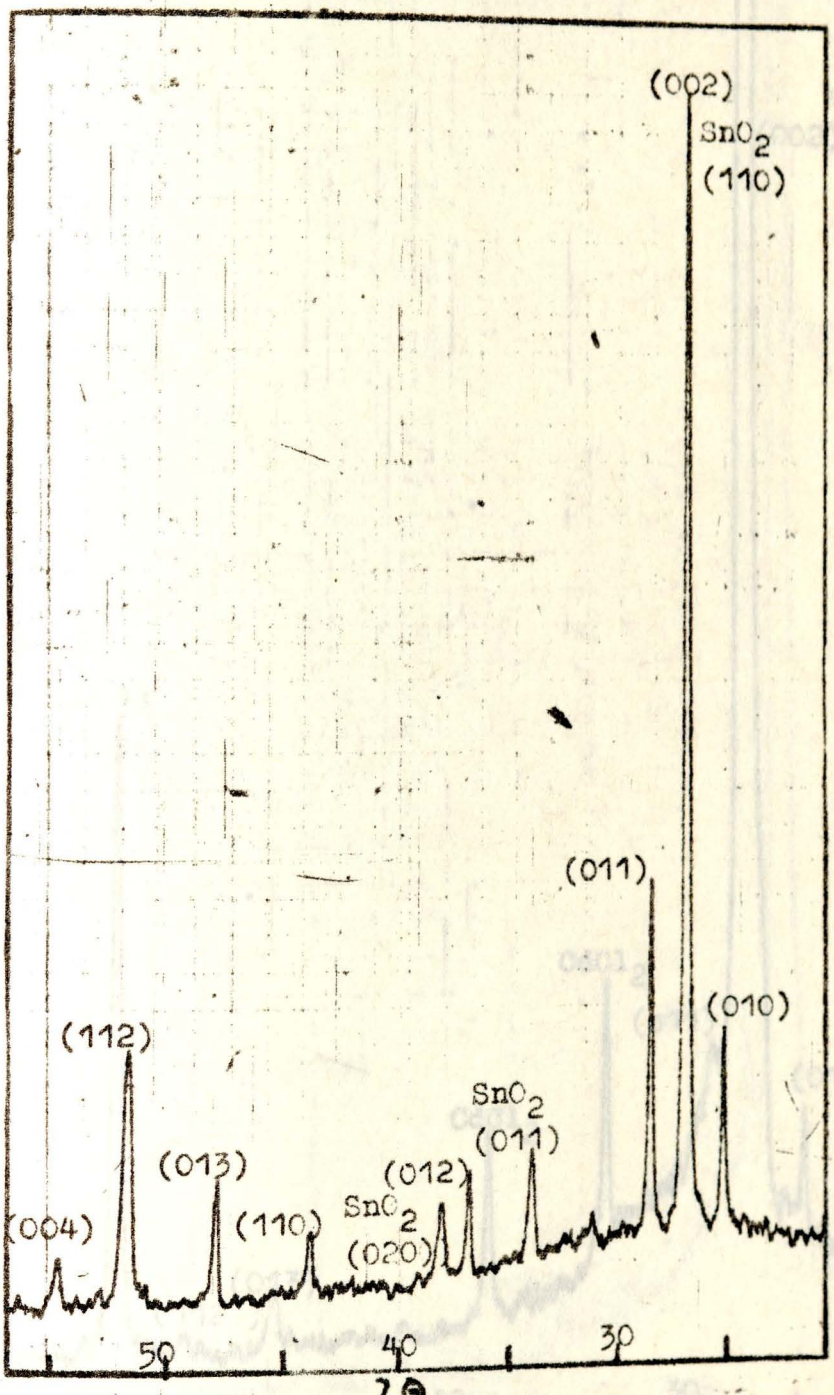


Fig. 19. XRDP of evaporated CdS film on SnO_2-coated glass slide

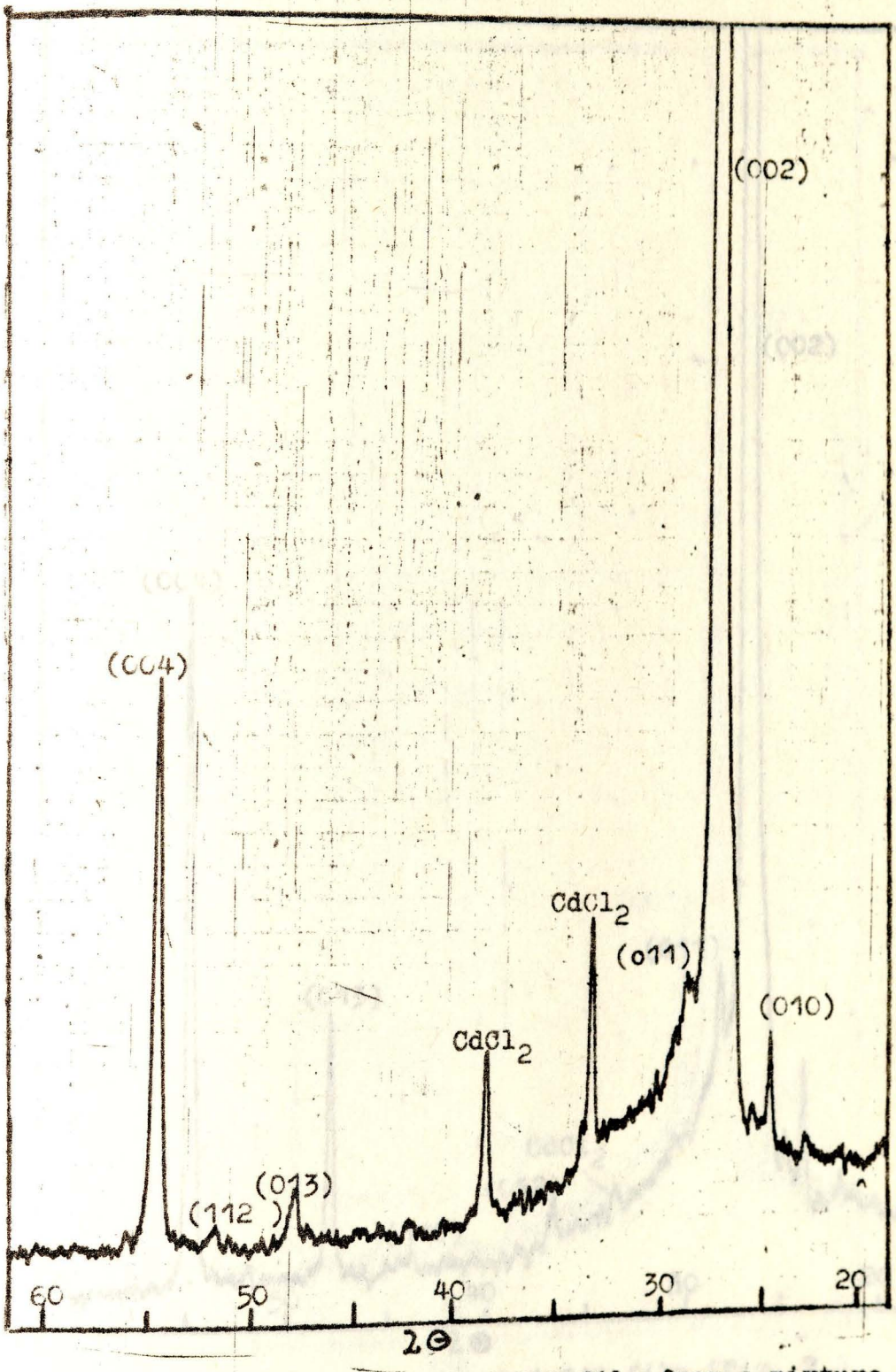


Fig. 20. XRDP of evaporated CdS film from a mixture of CdS and $CdCl_2$ on a glass slide

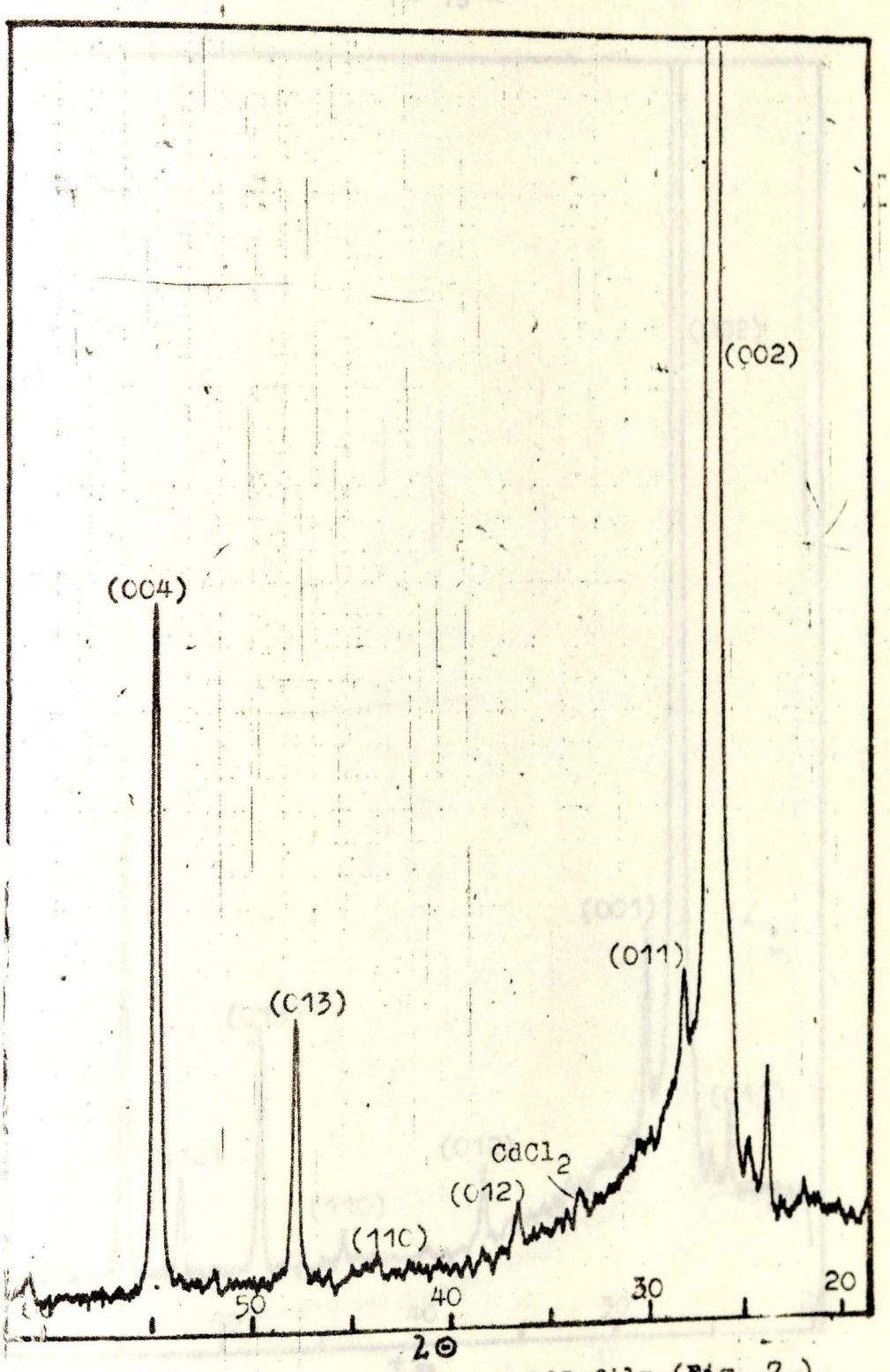


Fig. 21. XRDP of evaparated CdS film (Fig. 7.) after a certain heat treatment

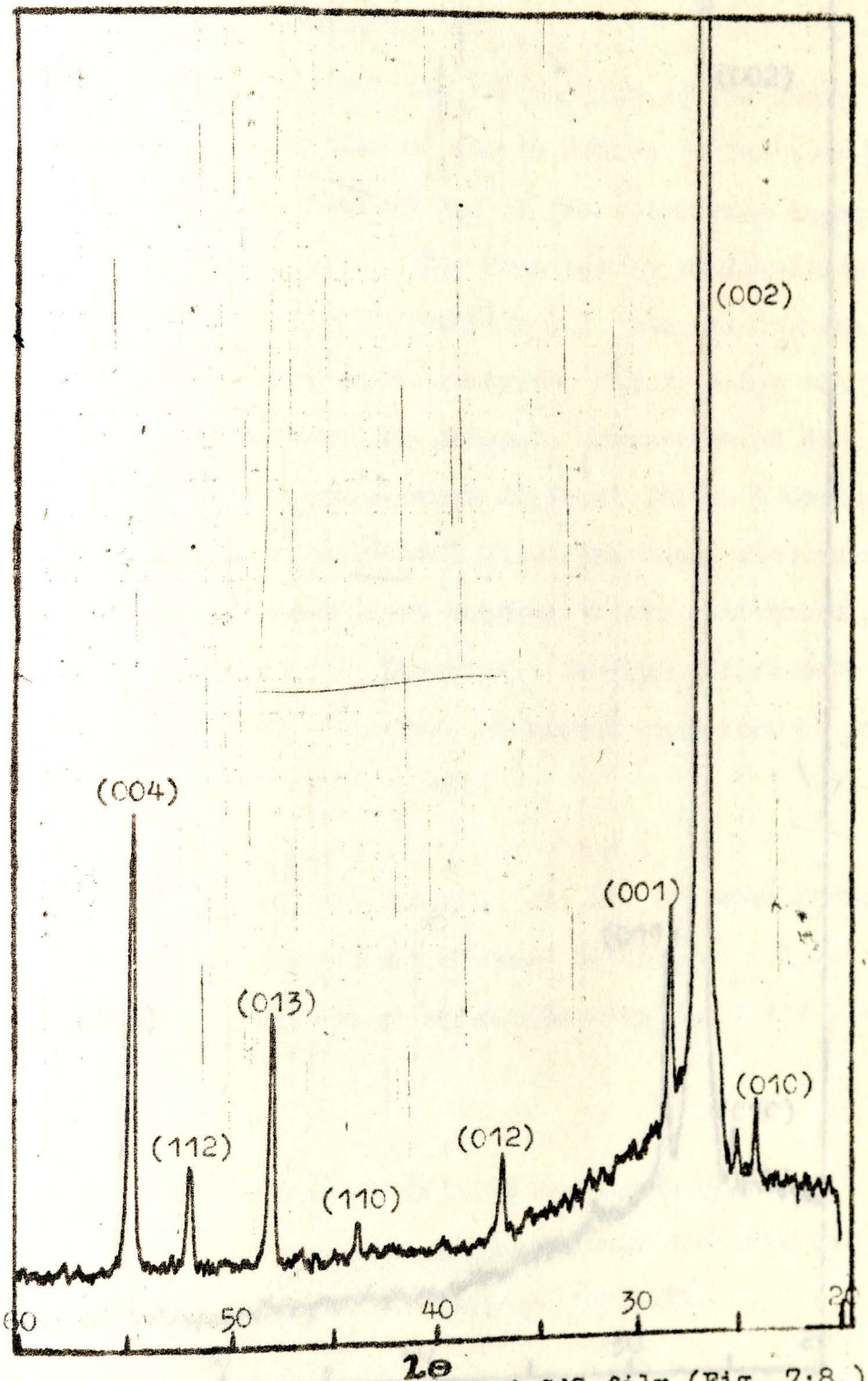


Fig. 22. XRDP of evaporated CdS film (Fig. 7;8.) after additional heat treatment

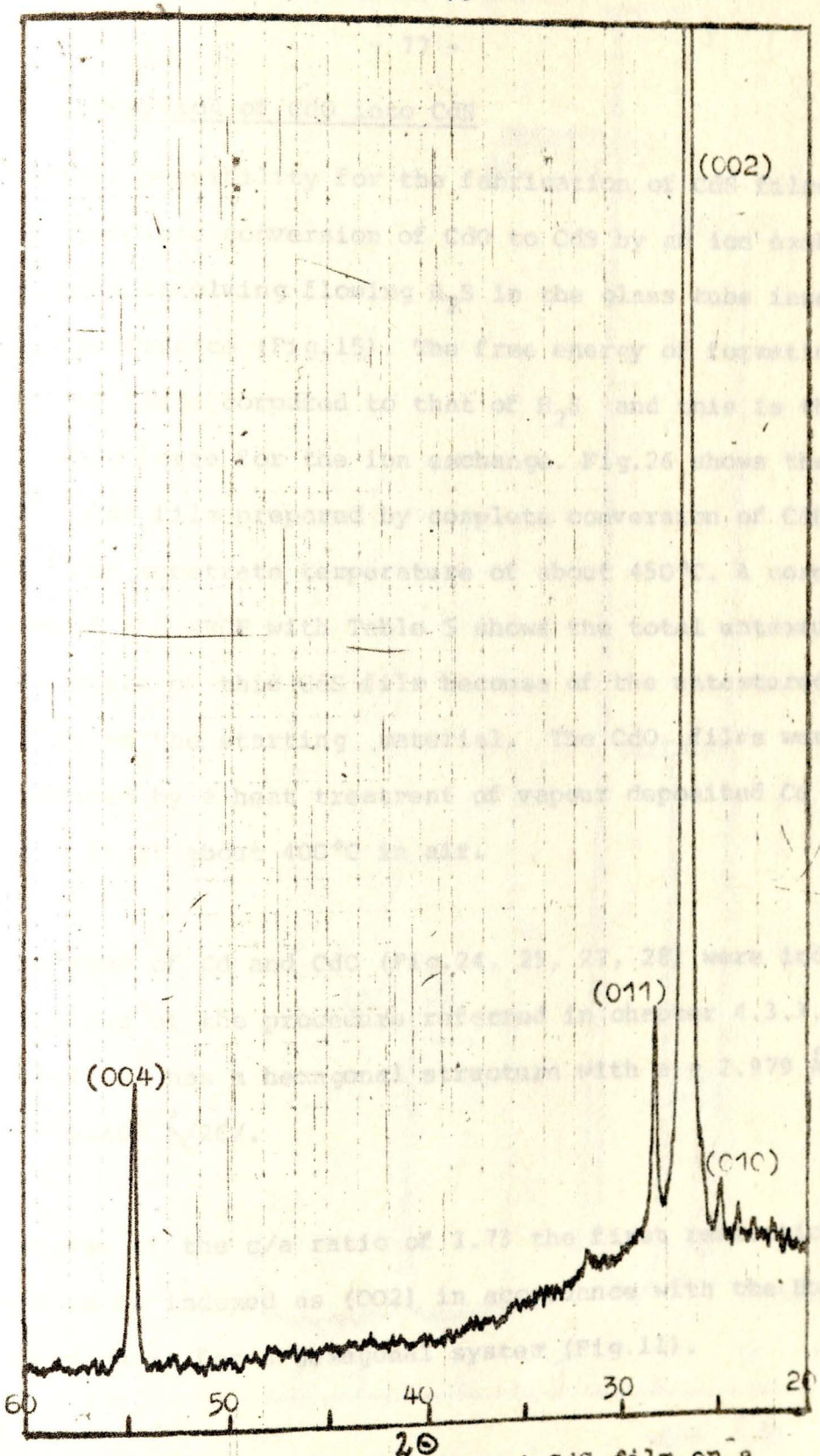


Fig. 23. XRDP of a evaporated CdS film on a heated glass slide

5.4.1.3 Conversion of CdO into CdS

Another possibility for the fabrication of CdS films is the complete conversion of CdO to CdS by an ion exchange process involving flowing H_2S in the glass tube inserted in the furnace (Fig.15). The free energy of formation of H_2O is large compared to that of H_2S and this is the driving force for the ion exchange. Fig.26 shows the XRDP of a CdS film prepared by complete conversion of CdO into CdS for substrate temperature of about 450°C. A comparison of the XRDP with Table 5 shows the total untextured structure of this CdS film because of the untextured CdO film as the starting material. The CdO films were produced by a heat treatrent of vapour deposited Cd layers (5.1.1) at about 400°C in air.

The XRDP of Cd and CdO (Fig.24, 25, 27, 28) were indexed by means of the procedure referred in chapter 4.3.3. and 4.3.1. Cd has a hexagonal structure with a = 2.979 Å and C = 5.168 Å/26/.

Because of the c/a ratio of 1.73 the first reflection has to be indexed as (002) in accordance with the Hull-Davey chart for a hexagonal system (Fig.11).

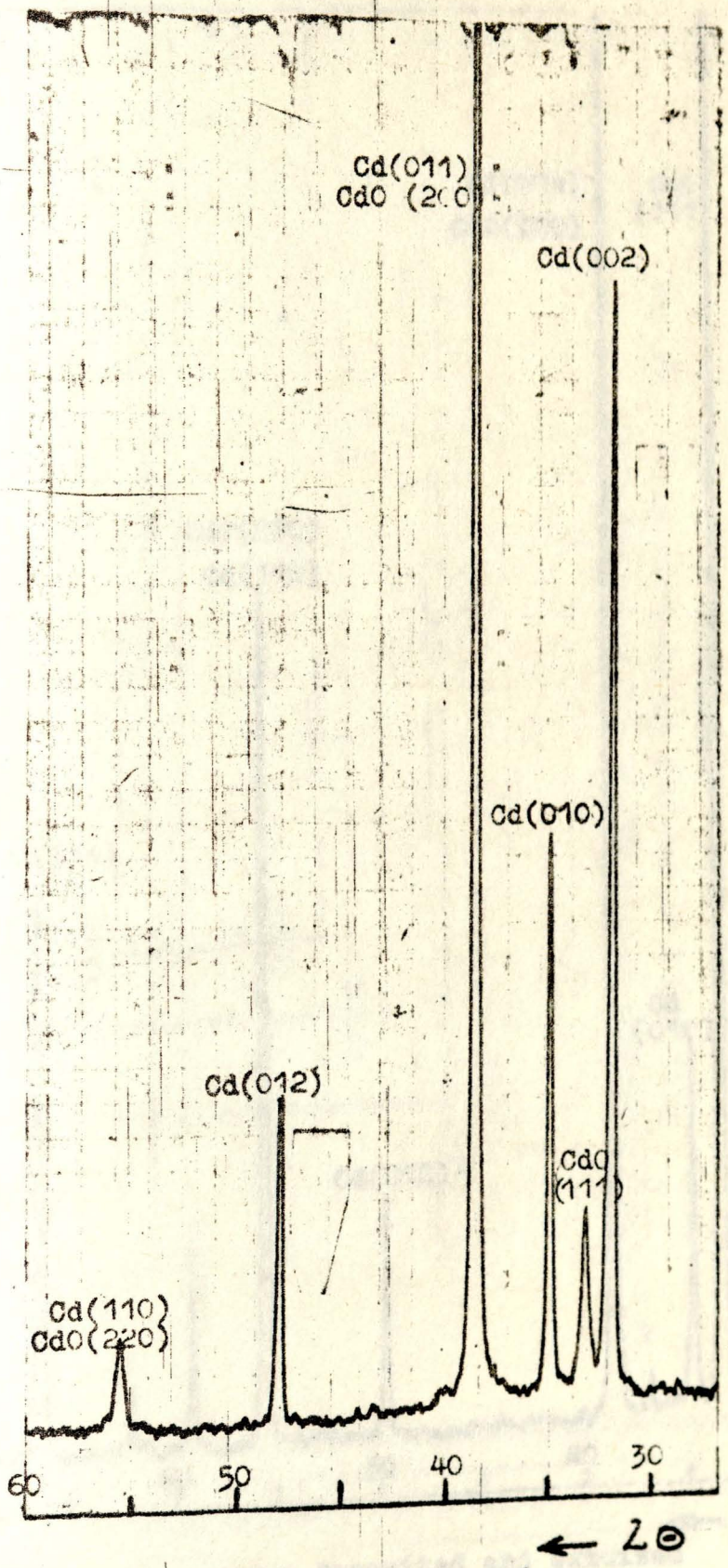


Fig. 24. XRDP of a vapour deposited and partly oxidized Cd film

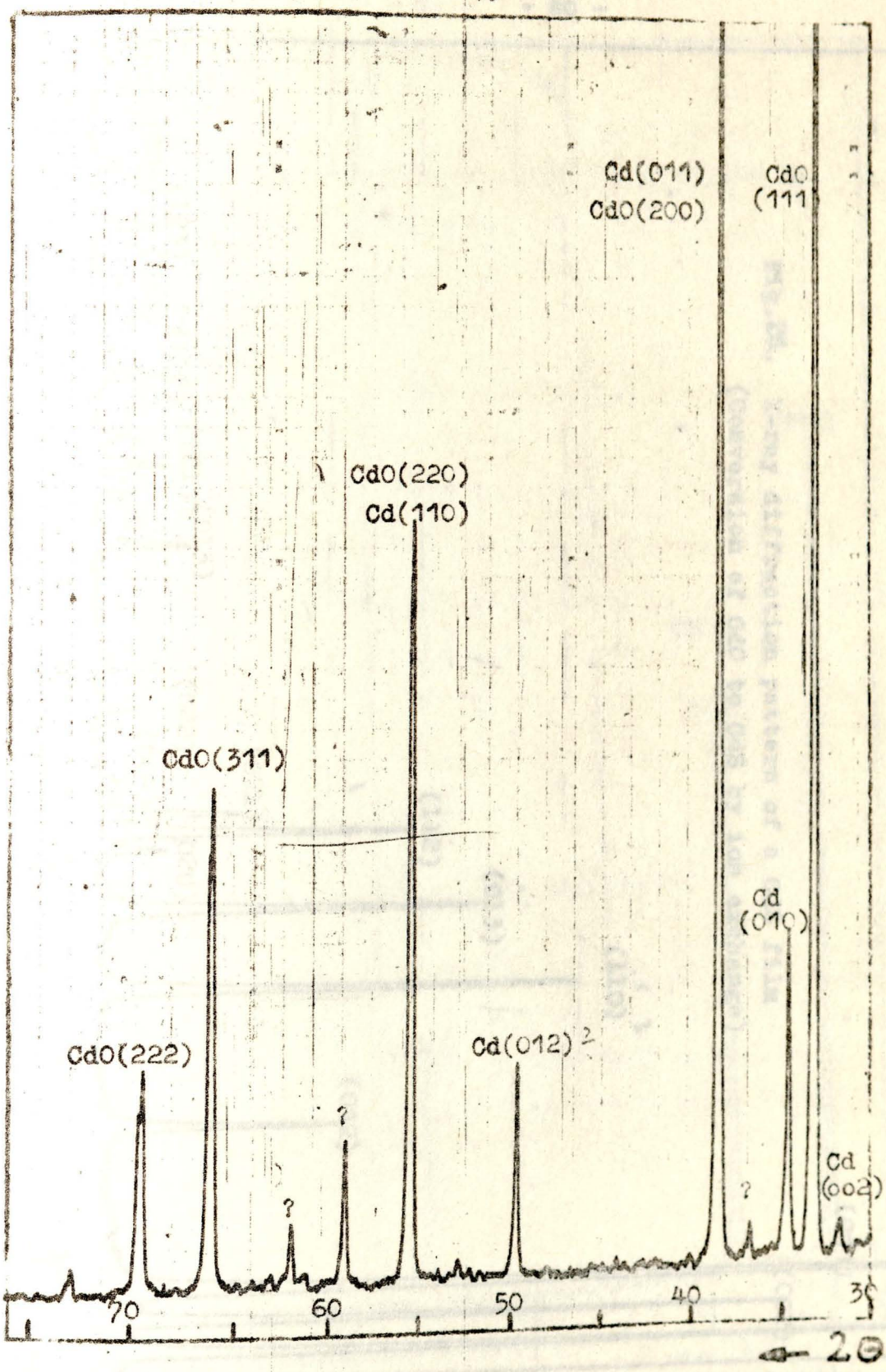


Fig. 25. XRDP of a vapour deposited and oxidized Cd film.

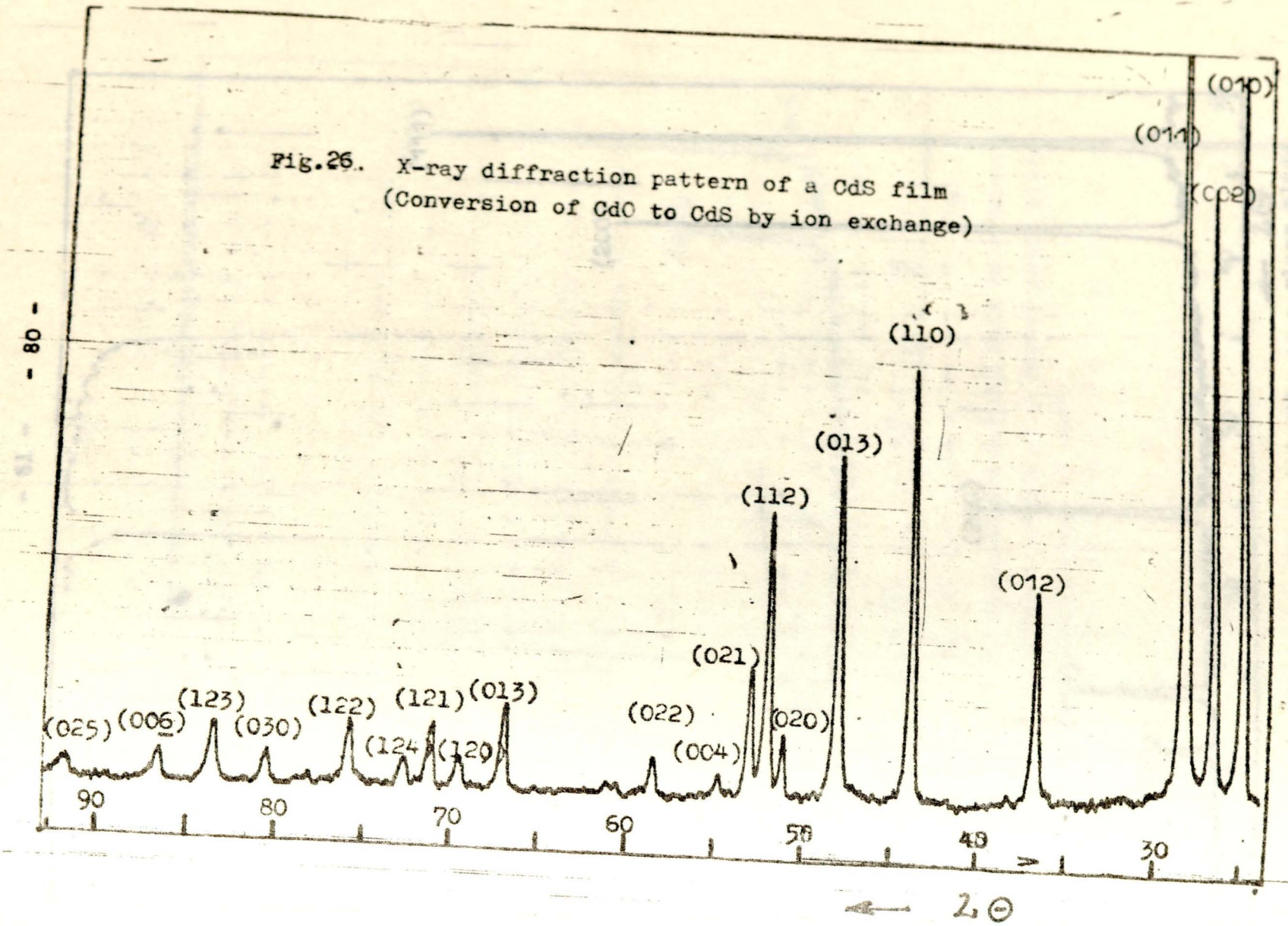


Fig.26. X-ray diffraction pattern of a CdS film
(Conversion of CdO to CdS by ion exchange)

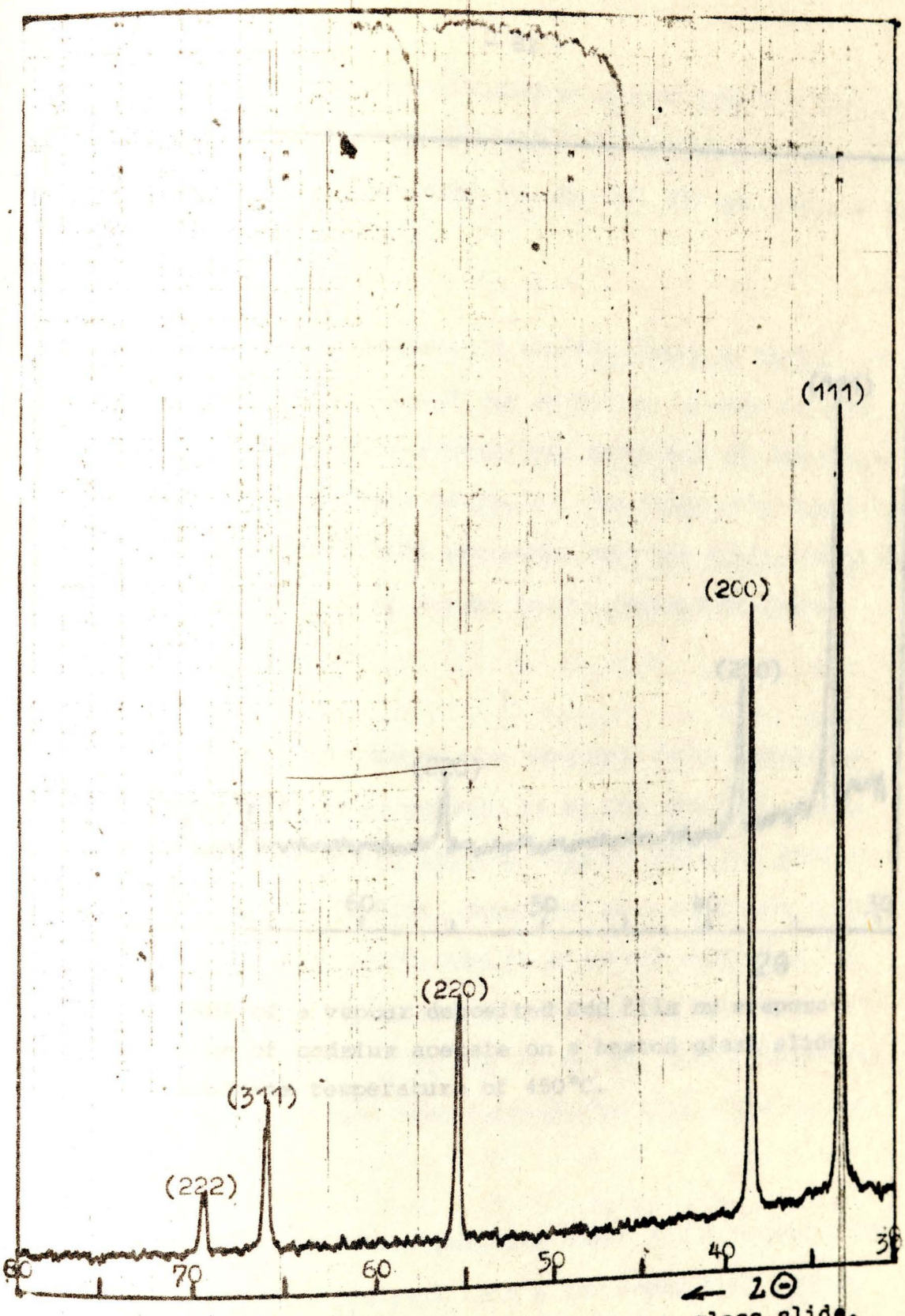


Fig. 27. XRDP of evaporated CdO film on a glass slide. (evaporation of cadmium acetate)

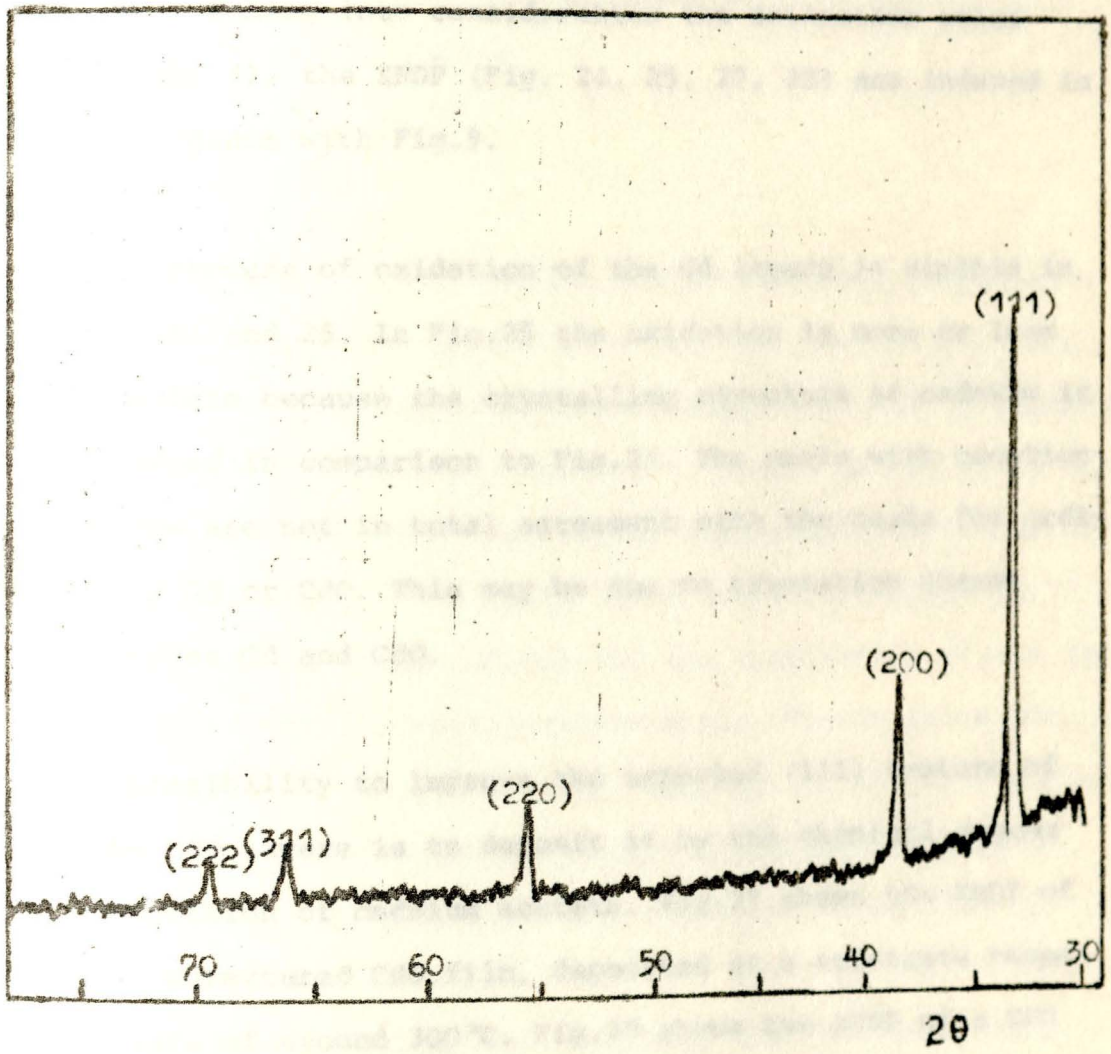


Fig.28. XRDP of a vapour deposited CdO film by evaporation of cadmium acetate on a heated glass slide subtrate temperature of 450°C.

CdO has a cubic face-centered structure with a = 4.811 A /26/. Taking into consideration the extinction rules (Table 4), the XRDP (Fig. 24, 25, 27, 28) are indexed in accordance with Fig.9.

The process of oxidation of the Cd layers is visible in Fig.24 and 25. In Fig.25 the oxidation is more or less complete because the crystalline structure of cadmium is changed in comparison to Fig.24. The peaks with question marks are not in total agreement with the peaks for ordinary Cd or CdO. This may be due to transition phases between Cd and CdO.

A possibility to improve the expected (111) texture of the CdO layers is to deposit it by the chemical vapour deposition of cadmium acetate. Fig.27 shows the XRDP of an untextured CdO film, deposited at a substrate temperature of around 300°C. Fig.28 shows the XRDP of a CdO layer deposited at about 500°C. Comparing the ratios of intensities I_{111}/I_{200} in Fig.27 and 28, it is found that for higher substrate temperatures the (111) texture improves.

Maruska et al /15/ have prepared their (111) textured CdO layers by spray pyrolysis onto glass substrates kept at temperatures of about 500°C. In the case of chemical vapour

deposition in a vacuum of 80 Pa, done here, a higher substrate temperature is necessary for getting (111) textured CdO layers.

5.4.2 Cu_xS - Films

The solid state reaction was sued for the preparation of Cu_xS layers on CdS layers (3.2.4. and 5.1.2). $CuCl/CuCl_2$ (mixture) films were deposited on CdS by evaporation of $CuCl/CuCl_2$ (mixture) powder in the glass tube at a vacuum of 80 Pa. If the substrate terperature was around 500°C, the solid state reaction between $CuCl/CuCl_2$ (mixture) and CdS and the evaporation of the produced $CdCl_2$ occurs simultaneously. Fig.29 shows the result of the solid state reaction. In comparison with x-ray data for different crystallographic phases of Cu_xS/25, 27/ the structure was found to be that of pseudocubic digenite (Table 6), which is not the efficient composition for CdS/Cu_xS photovoltaic cells.

An XPDP of the $CuCl/CuCl_2$ (mixture) powder used as an evaporant for the CuCl film deposition shows (Fig.30) that this powder is infact a mixture of CuCl and $CuCl_2$. CuCl has a cubic face-centered lattice structure with $a = 5.406$ Å (/26/, Tab.7). $CuCl_2$ is monoclinic with $a = 6,70$ Å, $b = 5,30$ Å, $c = 6,85$ Å and $\beta = 121°$ (/26/, Tab.8).

The evaporated layer of this powder showed a higher percentage of CuCl (Fig.31), and $CuCl_2$ as the reraining part which only allows the growth of digenite ($Cu_{1,8}S$, Fig.29).

A chemical purification of the $CuCl/CuCl_2$ (mixture) powder was necessary in decreasing the percentage of $CuCl_2$ in the deposited films (Fig.32). With this $CuCl/CuCl_2$ layer the solid state reaction produces a Cu_xS, in which the main part is the tetragonal $C_{1,96}S$ (Tab.9) but a certain amount of the orthorhombic Cu_2S (Tab.10) is present, too. Because of the high temperature solid state reaction $CuCl/CuCl_2$ (mixture) and CdS, high temperature modification of the tetragonal $Cu_{1,96}S$ appears (/2/, Tab.1). For conversion of CdS into Cu_xS at low temperature modification of $Cu_{1,96}S$, djurleite, has been found /28/.

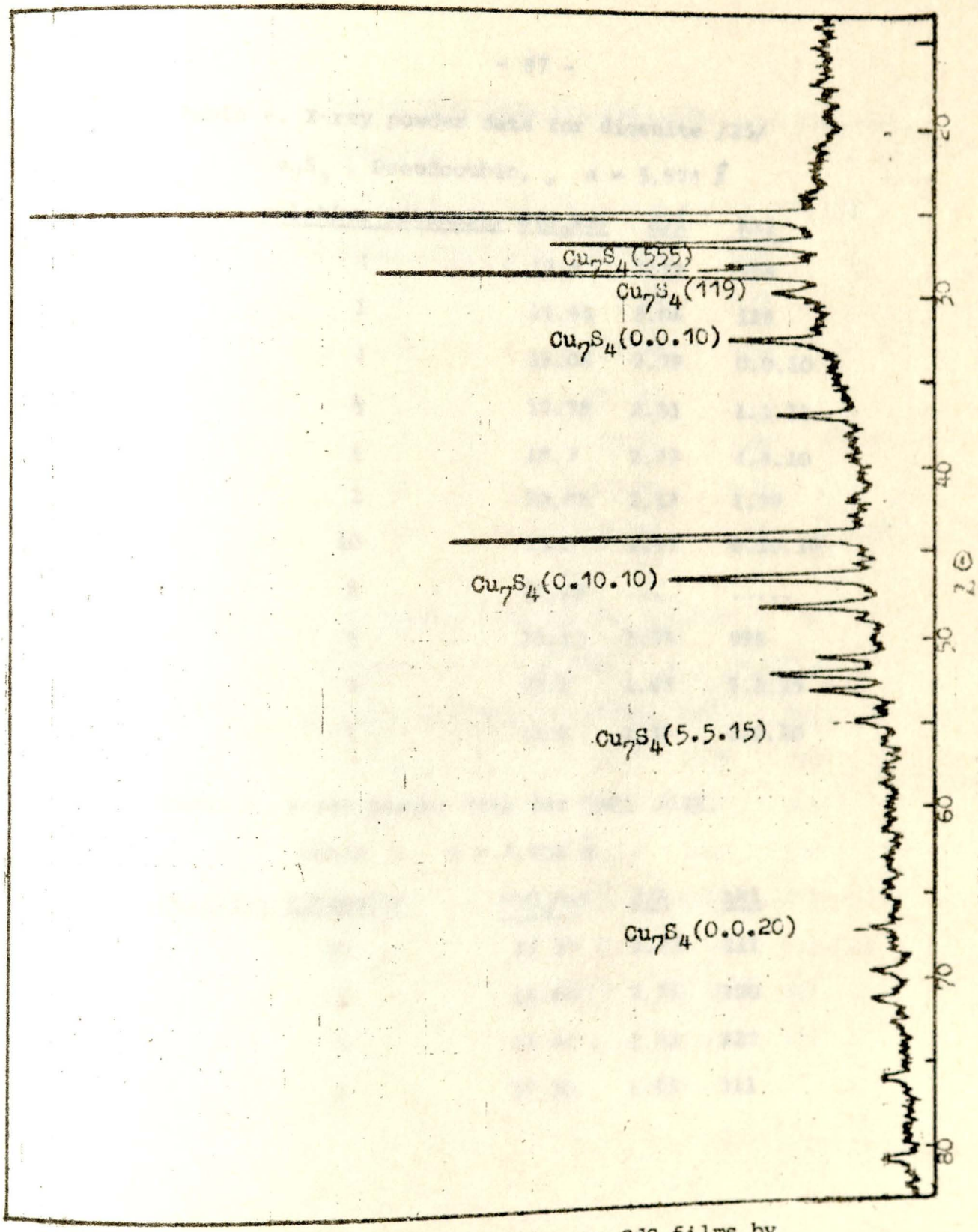


Fig.29. Production of Cu_xS films on CdS films by solid state reaction with an evaporated $CuCl/CuCl_2$ (mixture) film, XRDP.

Table 6. X-ray powder data for digenite /25/

Cu_7S_4 , Pseudocubic, , a = 5.571 Å

relative intensity	$\theta(C_uK\alpha)$	d/Å	hkl
4	13.9	3.22	555
1	14.65	3.06	119
4	16.05	2.79	0.0.10
½	17.75	2.51	1.1.11
½	18.7	2.43	4.4.10
1	20.85	2.18	1.99
10	23.0	1.97	0.10.10
½	24.25	....	.....
½	25.65	1.79	999
3	27.2	1.68	5.5.15
1	33.5	1.39	0.0.20

Table 7. X-ray powder data for CuCl /27/.

cubic , a = 5.406 Å

relative intensity	$\theta(C_uK\alpha)$	d/A	hkl
10	14.30	3.13	111
1	16.60	2.71	200
6	23.84	1.92	220
3	28.30	1.63	311

Table 8. X-ray powder data for $CuCl_2$/26/

monoclinic

a = 6,70 Å, b = 5.30 Å, c = 6.85 Å β = 121

relative intensity	Θ(CuKα)	d/Å
10	7.80	5.7
1	11.13	4.01
4	12.90	3.46
7	15.50	2.90
1	16.90	2.66
7	19.14	2.36

Table 9. X-ray powder data for $Cu_{1,96}S$/27/

Tetragonal , a = 3,99Å , c = 11,287 Å

relative intensity	Θ(CuKα)	d/Å	hkl
1	11.8	3.77	101
2	13.6	3.27	102
2	15.8	2.83	110
1	15.9	2.81	004
10	16.3	2.74	111,103
8	19.5	2.30	104
4	22.7	1.99	114

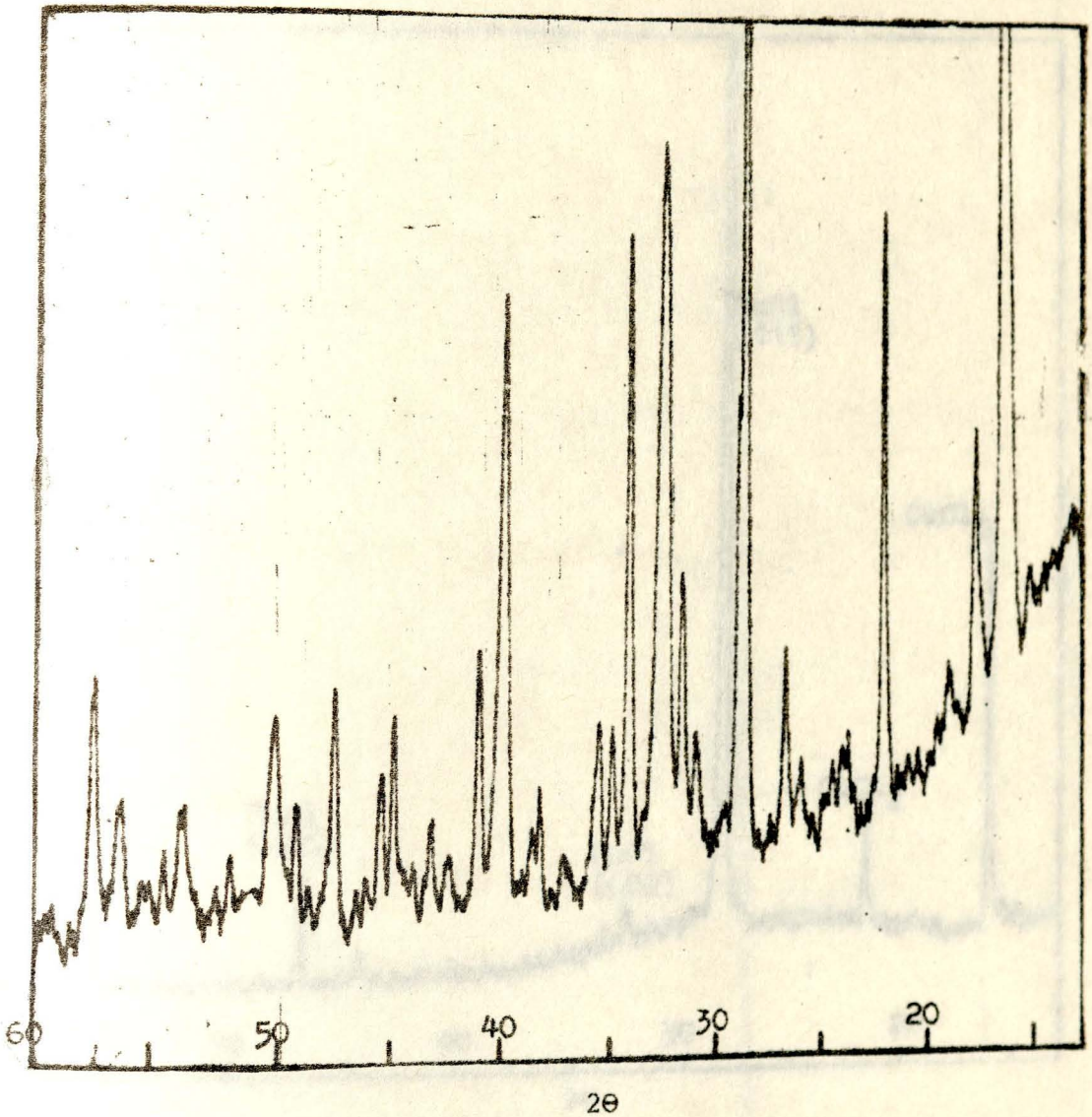


Fig.30. XRDP of the $CuCl/CuCl_2$ powder, which has been used as evaporant for CuCl layer deposition (see Fig.16).

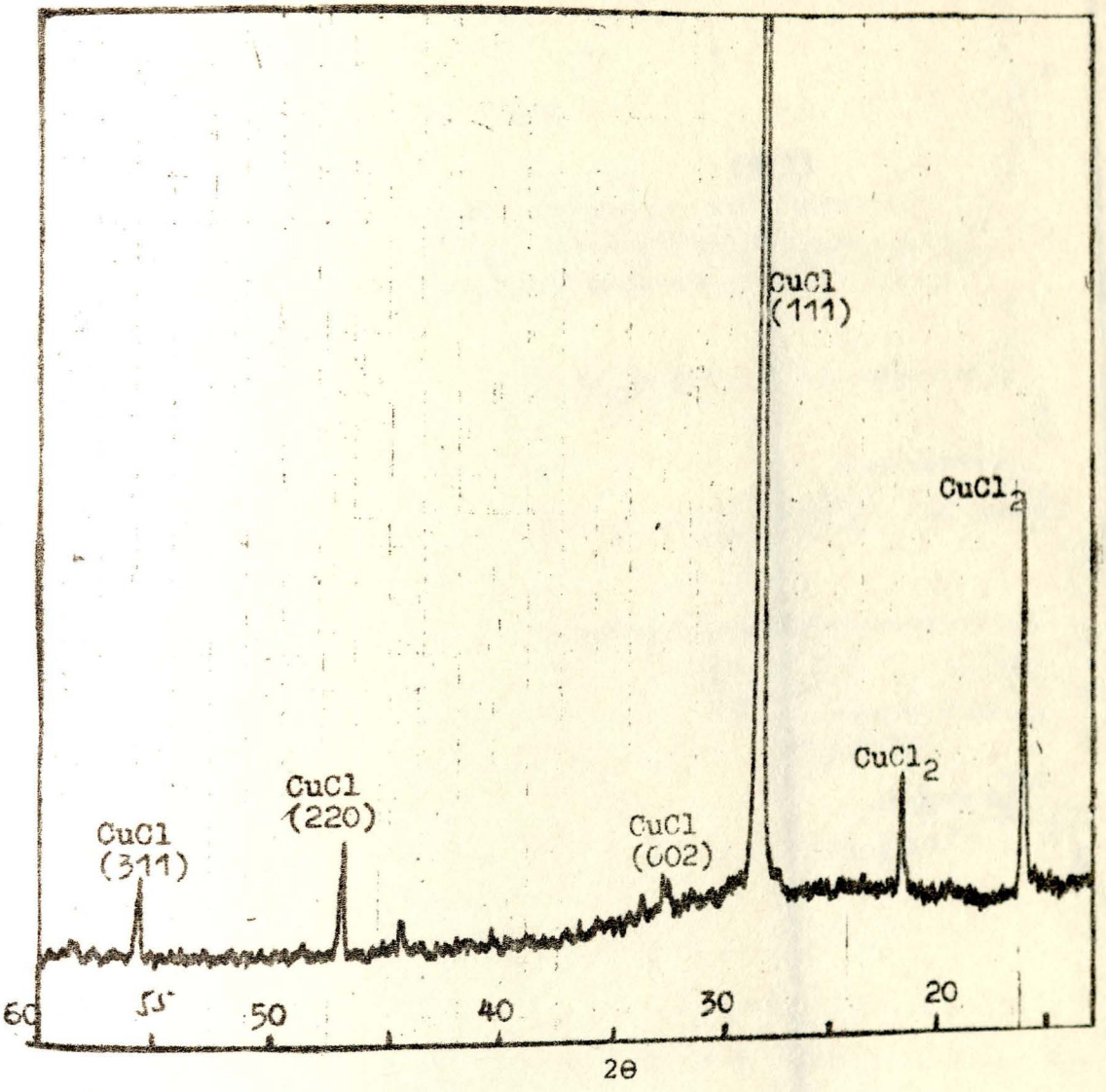


Fig.31. XRDP of the $CuCl/CuCl_2$ layer for solid state reaction (see Fig.29).

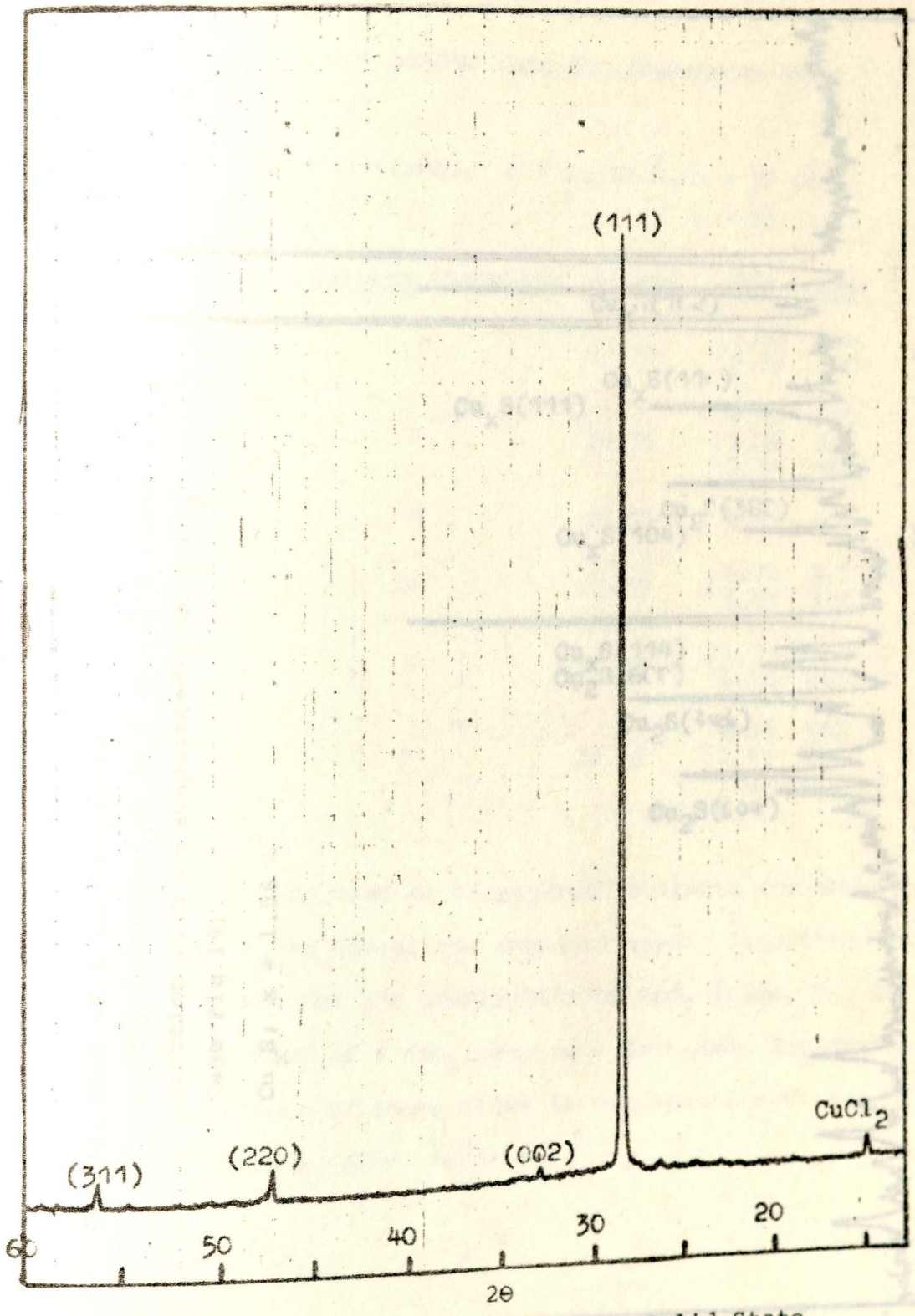


Fig.32. XRDP of the $CuCl/CuCl_2$ layer for Solid State reaction after reduction of the evaporant

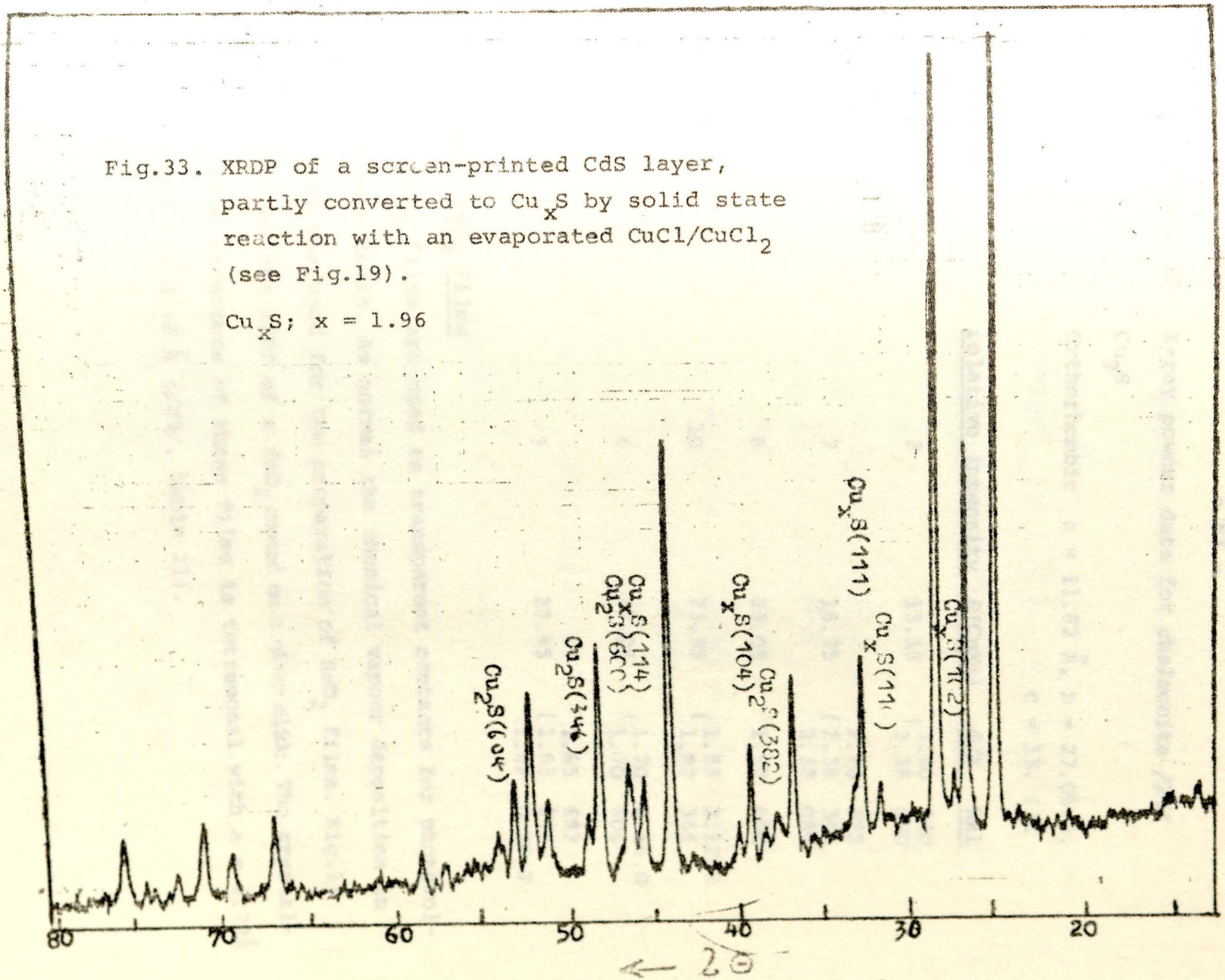


Fig.33. XRDP of a screen-printed CdS layer, partly converted to Cu_xS by solid state reaction with an evaporated $CuCl/CuCl_2$ (see Fig.19).

Cu_xS; x = 1.96

Table 10. X-ray powder data for chalcocite /25/

Cu_2S

Orthorhombic a = 11.82 Å, b = 27.05 Å, c = 13.43Å

relative intensity	Θ(CuKα)	d/Å	hkl
3	13.15	3.40	340
		3.38	080
7	18.75	2.40	382
		2.39	344
		2.38	084
8	23.05	1.97	600
10	23.35	1.88	3.12.2
		1.87	346
4	27.05	1.70	0.16.0
		1.70	604
?	27.95	1.65	682
		1.65	644
		1.64	0.16.2

5.4.3. SnO_2 Films

SnO_2 films are used as transparent contacts for photovoltaic cells. As normal the chemical vapour deposition in air was used for the preparation of SnO_2 films. Fig.18 shows the XRDP of a SnO_2 coated on a glass slide. The crystalline structure of these films is tetragonal with a = 4.73Å and c = 3.18 Å (/25/, Table 11).

Table 11. X-ray powder data for cassiterite /25/

SnO_2

Tetragonal a = 4.73 Å, c = 3.18 Å

relative intensity	Θ (CuKα)	d/Å	hkl
8	13.25	3.36	110
7	17.0	2.64	011
3	19.0	2.37	020
½	19.55	2.30	111
10	25.95	1.76	121
4	27.45	1.672	220

6. CONCLUSIONS AND OUTLOOK

The object of this study was to produce thin films for CdS/Cu_xS solar cells and to investigate their crystalline structure by x-ray diffraction.

It was found that the x-ray diffraction can be a valuable tool for the nondestructive characterization of both the CdS and Cu_xS films for CdS/Cu_xS solar cells.

Measurements of the degree of preferred orientation of the CdS layers and of the Cu_xS stoichiometry and phase structure can all be made on the same smaple in relation to the preparation and treatment conditions.

Further improvement of stoichiometry and structure of thin film CdS-based solar cells are expected by the use of other preparation conditions (high vacuum, high purity materials) ,and by the use of other materials (replacement of CuCl by CuI, replacement of Cu_xS by CdTe /29/).

An interesting method for the preparation of thin and pinhole free CdS films for the future is the conversion of CdO films to CdS /15/, especially the preparation of (111) textured CdO films at low temperatures as a starting material.

For the production of thin film solar cells with high efficiencies, the investigations by x-ray structure analysis have to be accompanied by measurements of electrical parareters of the films (resistivity, charge carrier nobility, photoconductivity etc.).

7. REFERENCES

1. D.C. Reynolds, Phys. Rev. 96 (1954) 1705.
2. W.R. Cook, Jr., L. Shiozawa, F. Augustine, J. Appl, Phys. 41 (1970) 3058.
3. M. Altmann, Elements of Solid State Energy Conversion, Van Nostrand Reinhold Company, New York, 1969.
4. A. Carlson, Research in semiconductor films, WADC. Tech. Rep. 56-62, 1956 (Clevite Corporation).
5. K.W. Böer,. J. Appl Phys. 50 (1979) 5356.
6. K.W. Böer, J. Cryst. Growth 59 (1982) 111.
7. S. Martinuzzi, Solar Cells 5 (1982) 243.
8. K. Radler, H. Frey, W. Müller, K. H. Schuller, J. Von Wienskowski, Thin Solid Films, 59 (1979) 13.
9. W. Müller, H. Frey, K. Radler, H. Schuller, Thin Solid Films, 59 (1979) 327.
10. H. Matsumoto, N. Nakayama, S. Ikegami, Jpn. J. Appl. Phys. 19 (1980) 129.
11. S. Martinuzzi, J. Oualid, F. Cabane-Brouty, A. Mostavan, J. Gervais, Rev. Phys. Appl. 14 (1979) 237.
12. M. Savelli, J. Bougnot, H. Luquet. M. Perotin, O. Maris, C. Gril, Solar Cells 5 (1982) 213.
13. H.L. Hwang, J.S. To, H.J. Ou, Y.K. Lee, C.Y. Sun, C.J. Chen, J.J. Loferski, Fifteenth IEEE Photovoltaic Specialists Conference 1981, Kissimee, FL, USA, 12-15 May, 1981 (New York USA IEEE, 1981) p.1035.

14. E.W. Williams, K. Jones, A.J. Griffiths, D.J. Roughley J.M., Bell, J.H. Steven and M.J. Huson, M. Rhodes, T. Costich, Sollar Cells 1 (1979/80) 357.

15. H.P. Maruska, A.R. Young II, C.R. Wronski, Fifteenth IEEE Photovoltaic Specialists Conference 1981, USA, 12-15 May, 1981 (New York, USA IEEE 1981) p.1034-4.

16. A. Baranski, W.R. Fawcett, A.C. Mc Donald J. Electrochem. Soc. 128 (1981) 963

17. M.K. Mukherjee, F. Pfisterer, C.H. Hewig, H.W. Schock, W. Bloss, J. Appl. Phys. 48 (1977) 1536.

18. F. Pfisterer, H.W. Schock, J. Wörner, Proc. 3rd Commission of European Communities Conf. on Photovoltaic Solar Energy, Cannes, October, 1980, Riedel, Dodrecht, 1980. p.762.

19. T.S. de Velde, J. Dieleman, Philips Res. Repts. 28 (1973) 573.

20. J.E. Marley, R.C. Dockerty, Phys. Rev. A140 (1965) 205.

21. E. Kawamata, Jpn. J. Appl. Phys. 21 (1982) 1243.

22. H. Lipson, H. Steeple, Interpretation of X-ray Powder Diffraction Patterns, Macmillan, London, 1970.

23. L.V. Azaroff, Elements of X-ray Crystallography, McGraw-Hill Book Comp., New York, 1968.

24. B.D. Cullity, Elements of X-ray Diffraction, Addison-Wesley Publishing Comp. Inc., Massachusetts, USA, 1959.

25. D.G. Berry, R.M. Thompson, X-ray Powder Data for Ore Minerals: The Peacock Atlas, Waverly Press, New York, 1962.

26. R.W.G. Wyckoff, Crystal Structures, John Wiley and Sons, New York, 1965.

27. ASTM: American Society: For Testing Materials: Cards: 4-0861, 12-205, 17-449, 20-365 (American Society of X-ray and Electron Diffraction, British Institute of Physics).

28. P.K. Roy, S.J. Luszcz, Fifteenth IEEE Photovoltaic Specialists Conference 1981, USA, 12-15 May, 1981 (New York, USA IEEE 1981) p. 1025-9.

29. H. Matsumoto, A. Nakano, H. Uda, S. Ikegami, T. Migazawa, Jpn. J. Appl. Phys. 21 (1982) 800.

DECLARATION

I, the undersigned, declare that this thesis is my original work and that all the sources of material used for the thesis have been duly acknowledged.

SALAH AHMED

PHYSICS DEPARTMENT

JUNE, 1983

DECLARATION

This thesis has been submitted for examination with my approval as the University Advisor.



DR. H.G. NEUMANN

JUNE, 1983